

# NATIONAL ADVISORY COMMITTEE FOR AERONAUTICS

TECHNICAL NOTE 4269

TRANSONIC DRAG OF SEVERAL JET-NOISE SUPPRESSORS

By Warren J. North

Lewis Flight Propulsion Laboratory  
Cleveland, Ohio



Washington

April 1958



TRANSONIC DRAG OF SEVERAL JET-NOISE SUPPRESSORS

By Warren J. North

SUMMARY

An experimental evaluation of the aerodynamic drag of several jet noise suppressors was conducted. The one-fifth scale suppressors were tested over a Mach number range from 0.65 to 1.10 at several nozzle pressure ratios.

The least drag was caused by the lobe-type suppressors. The eight-lobe nozzle with ejector caused the greatest drag.

The cruise propulsive-thrust loss of the tube nozzle and the eight-lobe nozzle with ejector should be about  $6\frac{1}{2}$  percent of the net thrust for the standard nozzle. The lobe nozzles and the standard nozzle with ejector should cause losses equivalent to 3 or 4 percent of the standard-nozzle net thrust.

INTRODUCTION

The high noise levels produced by turbojet engines have created a demand for exhaust noise suppressors with particular applicability to jet transport aircraft. A suitable noise suppressor should provide substantial noise reduction, should not introduce large internal or external aerodynamic losses, should be lightweight, should operate compatibly with thrust reversing devices, and should provide safe and trouble-free service.

A large research effort has been directed toward the design of effective noise-reducing nozzles. The internal aerodynamic losses of the most promising of these nozzles have not been prohibitively high. The external losses have received only very brief attention. Reference 1 gives the over-all aerodynamic performance of several full-scale suppressor nozzles at Mach numbers up to 0.5. Since the cruising Mach number of jet transports will be greater than 0.8, there is a need to determine the aerodynamic performance of noise-reducing nozzles at transonic Mach numbers. The purpose of the tests reported herein is

to obtain the transonic drag performance of several suppressor nozzles which are representative of the types currently being considered for jet transport application.

These tests were conducted with one-fifth scale suppressors over a range of Mach numbers from 0.65 to 1.10 and a range of nozzle pressure ratios from 1.0 to 6.0.

#### APPARATUS AND PROCEDURE

The Lewis 8- by 6-foot transonic and supersonic tunnel was used for the investigation. A photograph of the wind-tunnel perforated test section with the model and sweptforward support struts is shown in figure 1. The strut cross section was a 6-percent modified double-wedge airfoil. The model consisted of a conical forebody faired into a cylindrical nacelle with provision for interchangeable afterbodies and nozzles. Model fineness ratio was approximately 10. Exhaust flow was provided by ducting unheated pressurized air through the support struts.

In order to obtain the drag directly from a nulled strain-gage and bellows system, the model was constructed of two shells (fig. 2). The inner shell was grounded to the strut and absorbed the large thrust forces from the high-pressure jet. Only the outer shell was attached to the axial strain-gage system. This arrangement eliminated the necessity of obtaining external drag by subtracting a large thrust-minus-drag force from a large calculated thrust force.

The standard-nozzle afterbody and the suppressor configurations are shown in figure 3. All nozzles were designed with equal exit flow areas. The ejector configuration shown in figure 3(b) incorporates the standard primary nozzle. This is considered to be the cruise configuration of a variable-geometry nozzle which uses alternating inward and outward deflecting flaps on the primary nozzle for sound suppression during takeoff and initial climb. These photographs and sketches show the twin-shell arrangements with 1/16-inch annular clearance at the exit, which provided separation sufficient to prevent fouling. Since the pressure between the two shells differed slightly from the free-stream static pressure, it was necessary to apply corrections to the strain-gage-system drag data to compensate for the internal pressure forces.

In addition to the annulus pressure measurements, the models incorporated static-pressure instrumentation on the various afterbodies and the ejector. Jet total pressure was measured at a point upstream of the nozzle entrance as shown in figure 2.

The afterbody and ejector static-pressure instrumentation was used to separate the total drag into its component parts. The model forebody referred to herein includes the conical nose and the cylindrical body forward of station 65.7 (fig. 2). Forebody drag was obtained with the standard-nozzle configuration by subtracting afterbody pressure drag and friction drag from total drag. A friction drag coefficient of 0.003 (based on wetted area) was assumed. Forebody drag was invariant with afterbody and nozzle pressure ratio. Consequently, for the suppressor configurations the sum of the afterbody and ejector pressure, friction, and interference drags is the difference between the total and forebody drags. The internal shell of the eight-lobe nozzle expanded and fouled the outer shell during the ejector test and thereby affected the strain-gage measurements for this test only. It was necessary to obtain drag from pressure instrumentation for this configuration.

The test Mach numbers were 0.65, 0.80, 0.83, 0.86, 0.90, 1.00, and 1.10. At each Mach number the nozzle pressure ratio was varied over a range to include values compatible with turbojet-engine operation. All measurements were made with the model at zero angle of attack. The tunnel test-section static pressures and Reynolds numbers are shown in figure 4. The test Reynolds numbers (based on body length) are typical of those which are encountered with full-scale engine nacelles at cruising altitude. Test data were recorded and computed by the automatic data processing system discussed in reference 2.

## RESULTS AND DISCUSSION

### Total-Sound-Power Levels

The estimated total-sound-power levels of full-scale suppressors similar to the configurations discussed herein are shown in figure 5. These levels are estimated to be accurate to  $\pm 0.5$  decibel. The total-sound-power levels correspond to a thrust level of 7500 pounds. Determination of total-sound-power level involves an integration of the sound levels measured around an engine mounted in a free-field test stand and represents all the sound power emanating from the engine. These levels were obtained from reference 1, extrapolation of similar types from reference 1, and unpublished NACA data. The modified standard nozzle with ejector is the takeoff configuration of the variable-geometry nozzle mentioned previously. The suppressor nozzles produce total-sound-power levels which are from 2 to 8 decibels lower than that of the standard convergent nozzle. The best nozzle from a noise-suppression standpoint is the eight-lobe nozzle with ejector.

## Drag Results

In order to simplify the presentation of results and compare the various nozzles at realistic nozzle pressure ratios, an engine operating line was calculated by assuming constant turbine-outlet temperature. This operating line is presented in figure 6(b) as nozzle pressure ratio (nozzle total pressure divided by ambient static pressure) which is a function of flight Mach number.

For each nozzle the individual data points for total drag coefficient will be presented at various Mach numbers as a function of nozzle pressure ratio. A cross plot will then be presented which shows drag coefficients as a function of Mach number at the appropriate pressure ratios.

Standard nozzle. - The variation in total drag coefficient for the standard-nozzle installation as a function of nozzle pressure ratio and tunnel Mach number is shown in figure 6(a). For all test Mach numbers a decrease in drag coefficient occurs with increasing nozzle pressure ratio. The data points at a nozzle pressure ratio of approximately 1.0 are jet-off points. Figure 6(b) shows the total drag coefficient as a function of Mach number at the predetermined nozzle pressure ratios also shown in the figure. For comparative purposes the drag-rise Mach number is defined in this report as the Mach number at which the drag curve slope is 0.2. The drag rise for the standard nozzle then occurred at Mach number 0.86. This measurement of drag-rise Mach number was for a body of revolution with fineness ratio of 10 with no inlet flow and with interference effects from two sweptforward struts. The fineness ratio for the tunnel model was somewhat greater than that of an engine nacelle. However, because of engine-nacelle inlet flow, the maximum local Mach number on the nacelle should be similar to that on the tunnel model forebody.

The forebody (forward of station 65.7) drag coefficient  $C_{D,0}$  is also shown in figure 6(b). As mentioned in the section APPARATUS AND PROCEDURE this quantity was obtained by subtracting the afterbody pressure drag and friction drag from the total drag. The forebody drag was invariant with nozzle pressure ratio.

Standard nozzle with ejector. - The total drag coefficients, which were measured when the ejector was mounted on the standard nozzle, are shown in figure 7(a). There is no variation of drag coefficient with pressure ratio as was noted for the standard nozzle alone. The drag coefficients for the ejector model were higher than for the standard nozzle at all test conditions with a considerable increase above Mach 0.90. The component drags at flight nozzle pressure ratios are shown in figure 7(b). At Mach number 0.86 the total drag coefficient increased from 0.10 to 0.168 because of the addition of the ejector. Again the forebody drag curve was that which was obtained with the standard nozzle. The lower

curve, which represents the sum of forebody drag and afterbody pressure drag for the standard nozzle, indicates that thrust forces existed on the afterbody. When ejector pressure drag was added to the lower curve, the upper dashed curve resulted. The difference between the total drag curve and the top dashed curve should represent the afterbody friction and interference drag. Below a Mach number of 0.90 this difference is about 0.035. Above Mach number 0.90 there is a slight discrepancy between the component pressure drags and the strain-gage measured drag. The addition of the ejector caused no adverse effect on the drag-rise Mach number, which remained at 0.86.

Nine-tube nozzle. - As shown in figure 8(a) the drag coefficients for the nine-tube nozzle reach a maximum at a pressure ratio of 3.5 for all test Mach numbers. Low static pressures existed on the portion of the afterbody between the tubes and caused an increase in the drag. The cross plot in figure 8(b) shows that the total drag coefficient has a value of 0.16 at Mach number 0.86. This is 0.06 higher than the corresponding value for the standard-nozzle configuration. As in the case of the two previous nozzles, the drag rise occurs at Mach number 0.86.

Eight-lobe nozzle with centerbody. - There is a significant decrease in drag coefficient at the higher pressure ratios for the eight-lobe centerbody nozzle (fig. 9(a)). At Mach number 0.86 the total drag coefficient, as determined from figure 9(b) for the eight-lobe nozzle with centerbody, is 0.046 greater than that of the standard-nozzle configuration. The drag-rise Mach number again occurs at about 0.86.

Eight-lobe nozzle. - The open centerbody model was constructed with smaller afterbody cross sections than the centerbody lobed configuration. The external drag coefficients of the eight-lobe nozzle (fig. 10(a)) are similar to those of the centerbody lobe nozzle except that drags at a free-stream Mach number of 0.90 are smaller for the open centerbody configuration. For a pressure ratio of 4.23 the configuration without centerbody (fig. 10(b)) yielded a drag coefficient at Mach 0.90 which was 0.019 lower than that for the centerbody configuration (fig. 9(b)). The drag-rise Mach number was increased to 0.90 for the lobe configuration without centerbody.

Eight-lobe nozzle with ejector. - Since the strain-gage measurements were not available for this configuration (see APPARATUS AND PROCEDURE section), the total drag coefficient was obtained by a buildup of pressure drags and an extrapolation of friction and interference drag based on the standard-nozzle ejector configuration. Although figure 11(a) shows that the afterbody pressures produced a thrust force, the ejector pressure drags were large and the resulting over-all drags (fig. 11(b)) were greater than for the other configurations. The drag-rise Mach number was 0.80.

### Propulsive-Thrust Losses

The differences between the total drag coefficients for the suppressor models and the standard-nozzle configuration are shown in figure 12. Since the forebody drag at a given Mach number was invariant, these differences are attributed to the suppressors. The applicable engine operating line was previously shown in figure 6(b). In the Mach number range of jet transport interest (0.80 to 0.90) the lobe nozzle suppressors produced the least drag increase. At Mach number 0.86 the lobe nozzle with ejector caused nearly three times as much drag increase as the lobe nozzle without ejector. Ejector drag could be eliminated during cruising flight if the ejector were retracted and stowed in the nacelle after takeoff.

The drag increases at Mach number 0.86 were converted to percent of standard-nozzle net thrust and are shown in figure 13 as the shaded areas in the bar graph. The standard-nozzle net-thrust calculation was based on  $1\frac{1}{2}$ -percent nozzle total-pressure loss and airflow corrected to turbojet-exhaust temperature.

Nozzle thrust coefficients were assumed in order that over-all propulsive-thrust losses could be calculated. The lobe-nozzle thrust coefficients were assumed to be 1 percent less than that of the standard nozzle, and the coefficient for the tube nozzle was assumed to be  $2\frac{1}{2}$  percent less. These values were determined from total-pressure losses in full-scale suppressor nozzles. The thrust coefficient for the centerbody lobe nozzle was corrected for a small pressure force which acted on the centerbody in the drag direction. These thrust losses presented in terms of standard-nozzle net thrust are shown as the unshaded portions of the bar graph in figure 13.

The propulsive-thrust loss is the sum of the shaded and unshaded portions of the bar graph. The cruise propulsive-thrust loss for the tube nozzle and eight-lobe nozzle with ejector is about  $6\frac{1}{2}$  percent of the net thrust for the standard nozzle. The standard nozzle with ejector and the lobe nozzles will cause a 3- or 4-percent loss.

### Airplane Performance Penalties

The final choice of an effective jet-noise suppressor will depend largely upon the corresponding airline operating profits. A first-order approximation of operating profits is aircraft payload.

In order to maintain an economical altitude and retain the speed advantage for the jet transport, a decrease in propulsive thrust caused by a sound suppressor must be offset by increased engine power settings. This assumes, of course, that it is not feasible to redesign the engine and airframe. For a given altitude and airspeed the thrust specific fuel consumption is nearly constant throughout the range of power settings of interest. A suppressor propulsive-thrust loss, then, is converted into an equivalent percentage increase in fuel required. By neglecting suppressor weight and assuming that the aircraft is payload weight limited, the increased fuel requirements will displace an equivalent weight of payload. If one considers a long-range jet transport airplane cruising at Mach number 0.86 with a range of 3500 miles and a payload equivalent to 15 percent of gross weight, the percentage decrease in payload is approximately 2.8 times as great as the loss in propulsive thrust. This relation is shown in figure 14. For the suppressors tested the payload penalty varies from 9 to 18 percent.

#### CONCLUDING REMARKS

The preceding results indicate that the eight-lobe nozzle with ejector, which produced the least noise, caused the greatest drag. As mentioned previously, a retractable ejector would be desirable from the standpoint of drag reduction during cruise flight. The least suppressor drag was caused by the lobe nozzles.

The cruise propulsive-thrust loss for the tube nozzle or the eight-lobe nozzle with ejector should be about  $6\frac{1}{2}$  percent of the net thrust of the standard nozzle. The standard nozzle with ejector and the lobe nozzles should cause a 3- or 4-percent loss.

Although the previous drag results have been presented in terms of aircraft performance, it should be remembered that these tests were accomplished with a cold jet and without the presence of a wing.

The effect of increased jet temperature, simulating a turbojet exhaust, would be expected to have a uniformly small effect on the afterbody drag of the standard, lobe, and tube nozzles. Increased jet temperature will raise the ejector primary velocity and should cause a small increase in the secondary flow by nature of greater viscous-shear pumping. Although this increased secondary flow will cause a small reduction in the ejector pressure drag, it should increase the pressure and friction drag on the primary-nozzle afterbody. One might expect, then, an insignificant effect of primary-jet temperature upon the ejector configuration drag.

Interference effects involving the suppressor, a sweptback nacelle strut, and a nearby wing should increase the aircraft drag. Consequently, in terms of aircraft performance, these wind-tunnel tests should produce optimistic results.

On most medium and long-range flights the decrease in cruise propulsive thrust will be more critical than the decrease in takeoff thrust. For flights in which takeoff weight is limited by runway length, large thrust reductions due to seasonal temperature increases will be more serious than the moderate thrust loss due to a suppressor.

Lewis Flight Propulsion Laboratory  
National Advisory Committee for Aeronautics  
Cleveland, Ohio, February 24, 1958

## APPENDIX - SYMBOLS

A area,  $A_{\max} = 0.3491$  sq ft  
 $C_D$  drag coefficient,  $D/q_0 A_{\max}$   
D drag  
M Mach number  
p static pressure  
q dynamic pressure,  $0.7 \text{ pM}^2$

## Subscripts:

AB afterbody  
E ejector  
max maximum  
O free stream and model forebody  
t total

## REFERENCES

1. Ciepluch, Carl C., North, Warren J., Coles, Willard D., and Antl, Robert J.: Acoustic, Thrust, and Drag Characteristics of Several Full-Scale Noise Suppressors for Turbojet Engines. NACA TN 4261, 1958.
2. Staff of the Lewis Laboratory: Central Automatic Data Processing System. NACA TN 4212, 1958.

4858

CP-2



Figure 1. - Model installed in wind tunnel.

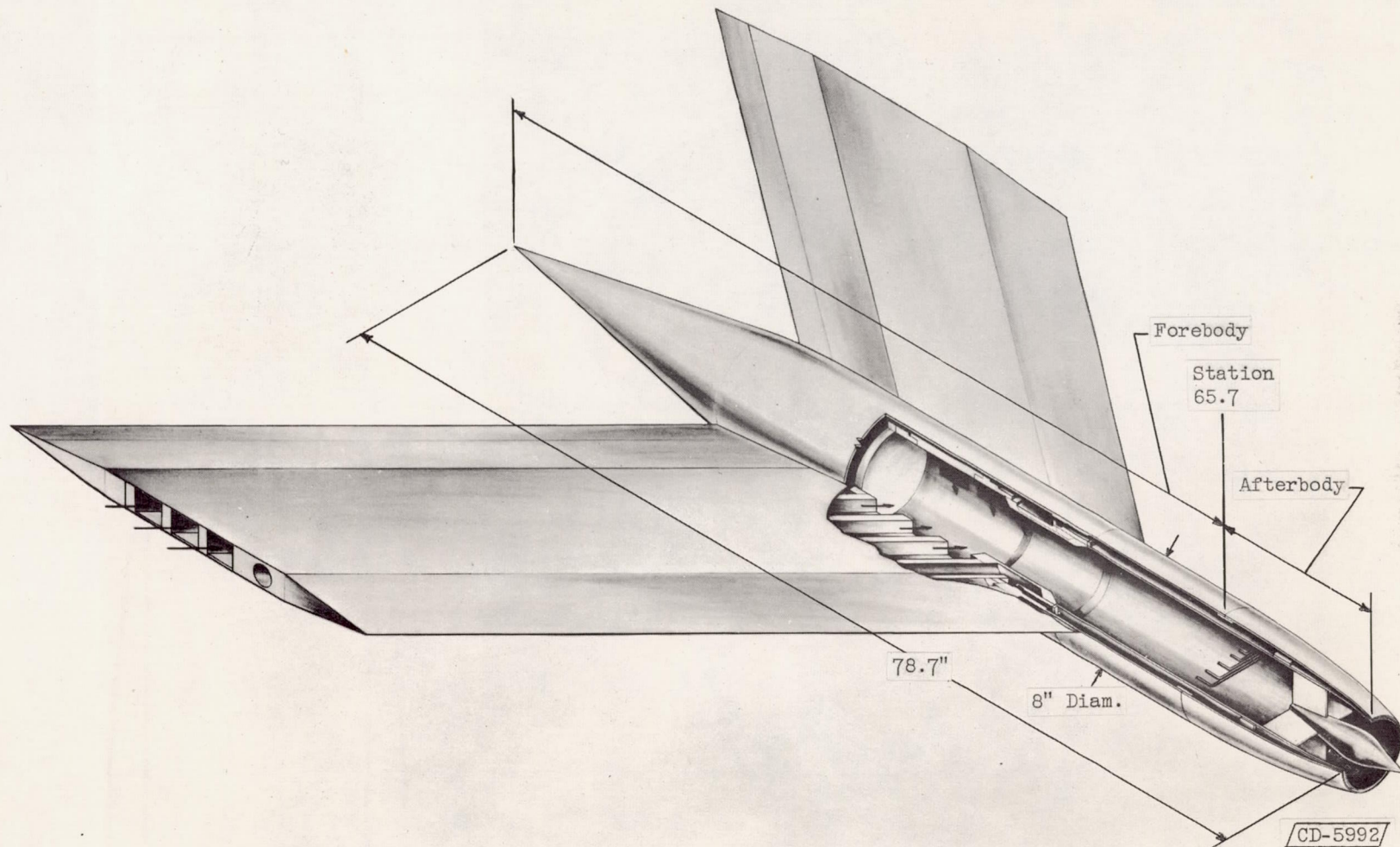
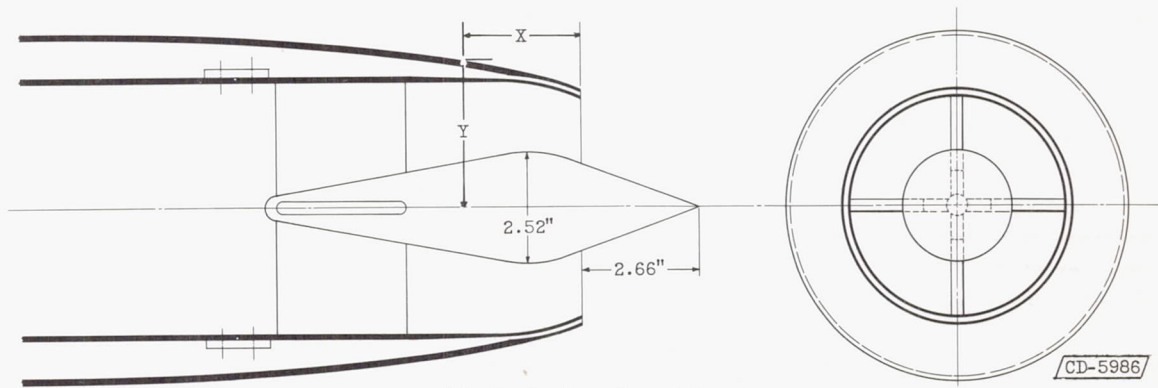
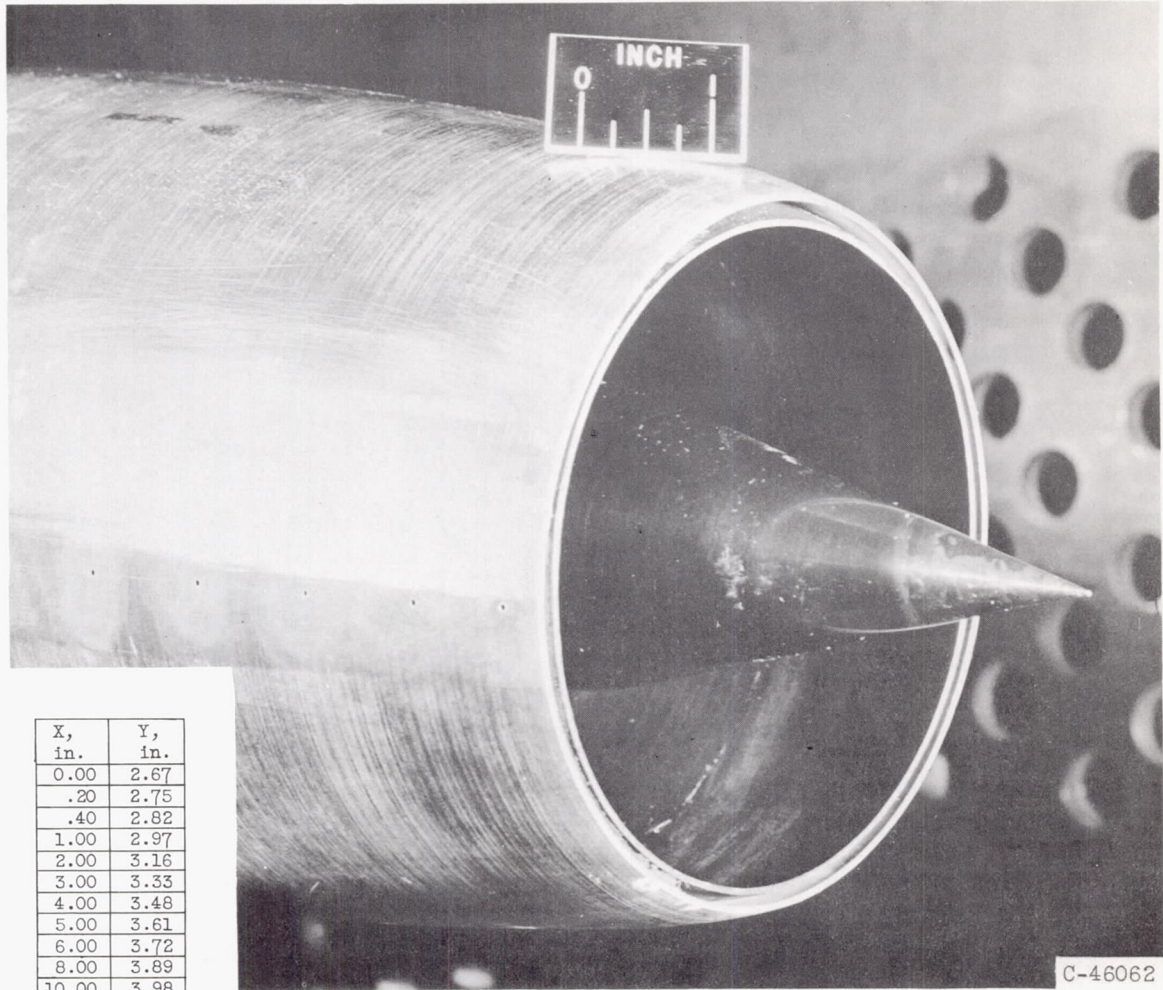


Figure 2. - Sketch of model assembly.

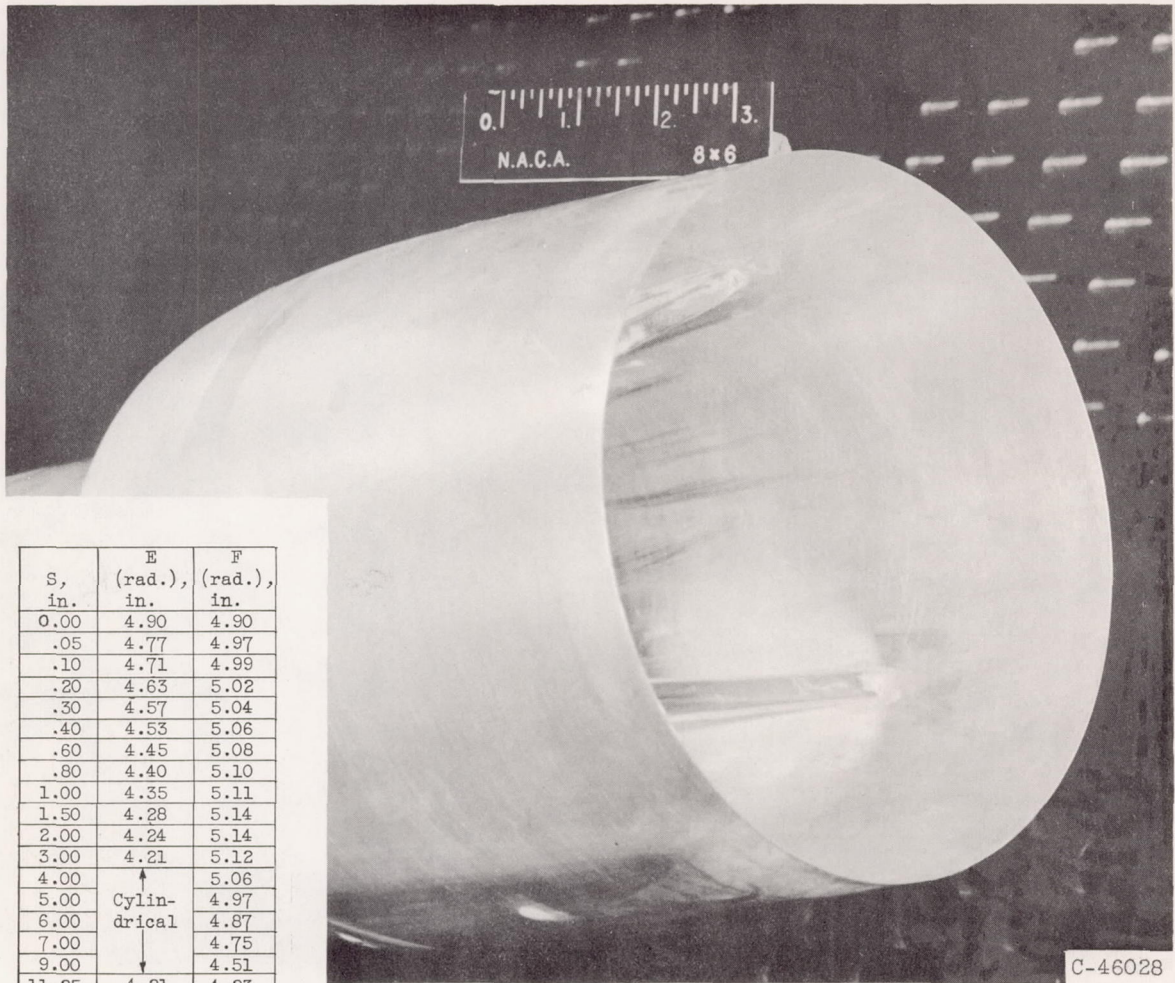


(a) Standard configuration.

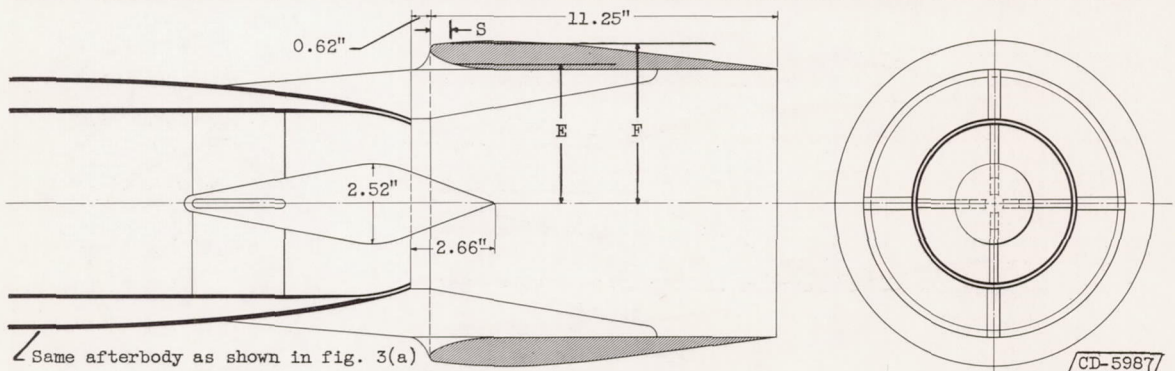
Figure 3. - Nozzle details.

CD-5986

4838



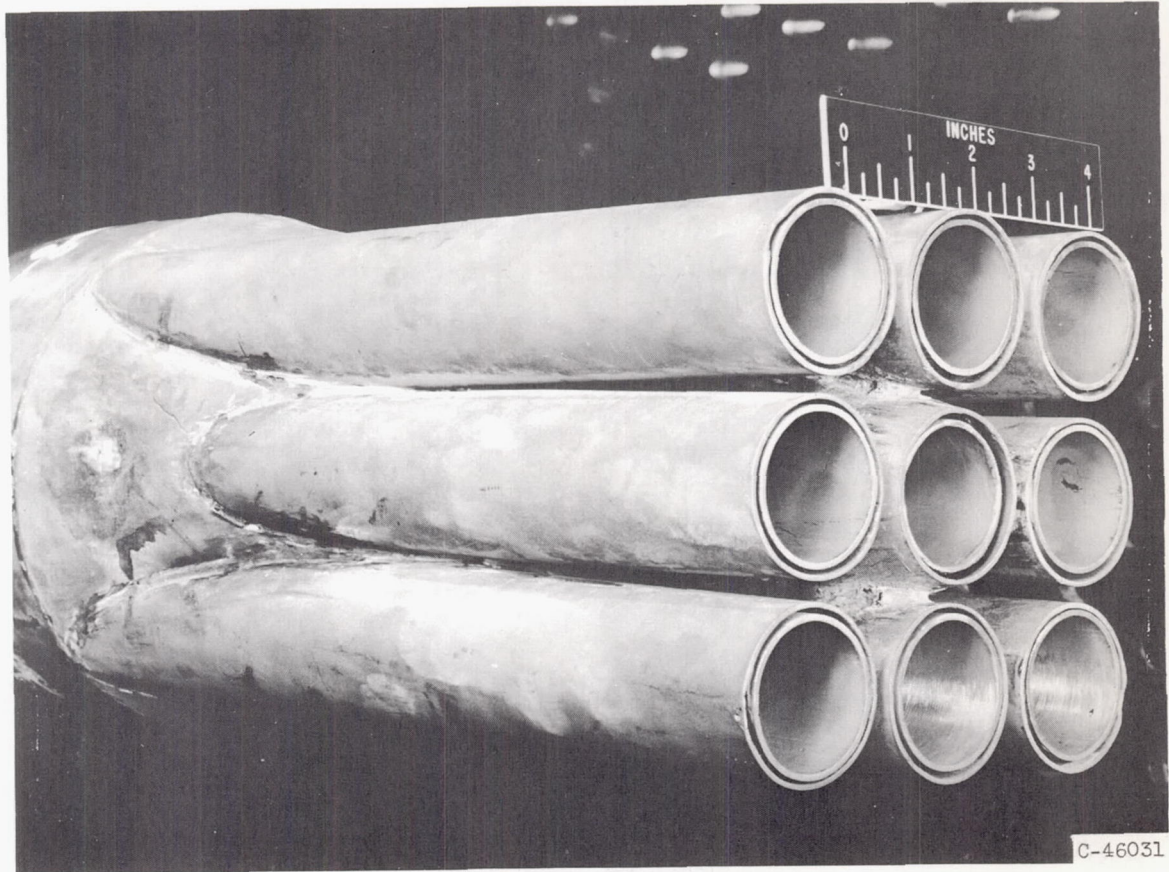
S, in.	E (rad.), in.	F (rad.), in.
0.00	4.90	4.90
.05	4.77	4.97
.10	4.71	4.99
.20	4.63	5.02
.30	4.57	5.04
.40	4.53	5.06
.60	4.45	5.08
.80	4.40	5.10
1.00	4.35	5.11
1.50	4.28	5.14
2.00	4.24	5.14
3.00	4.21	5.12
4.00		5.06
5.00	Cylindrical	4.97
6.00		4.87
7.00		4.75
9.00		4.51
11.25	4.21	4.23



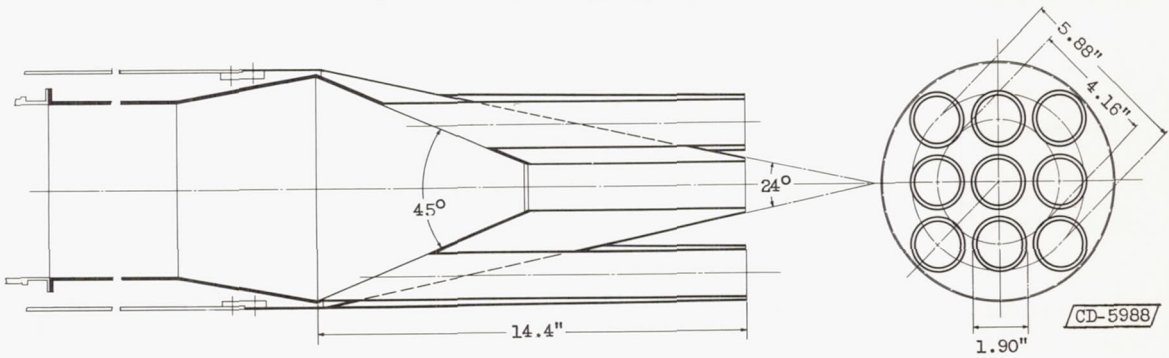
Same afterbody as shown in fig. 3(a)

(b) Standard nozzle with ejector.

Figure 3. - Continued. Nozzle details.



C-46031

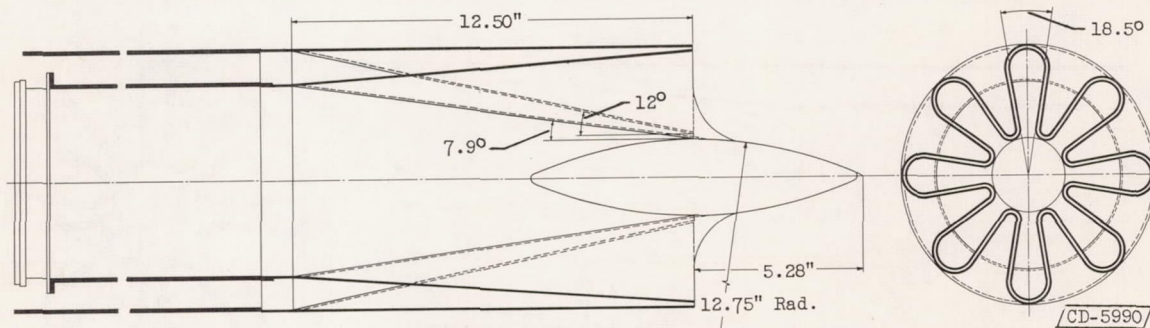
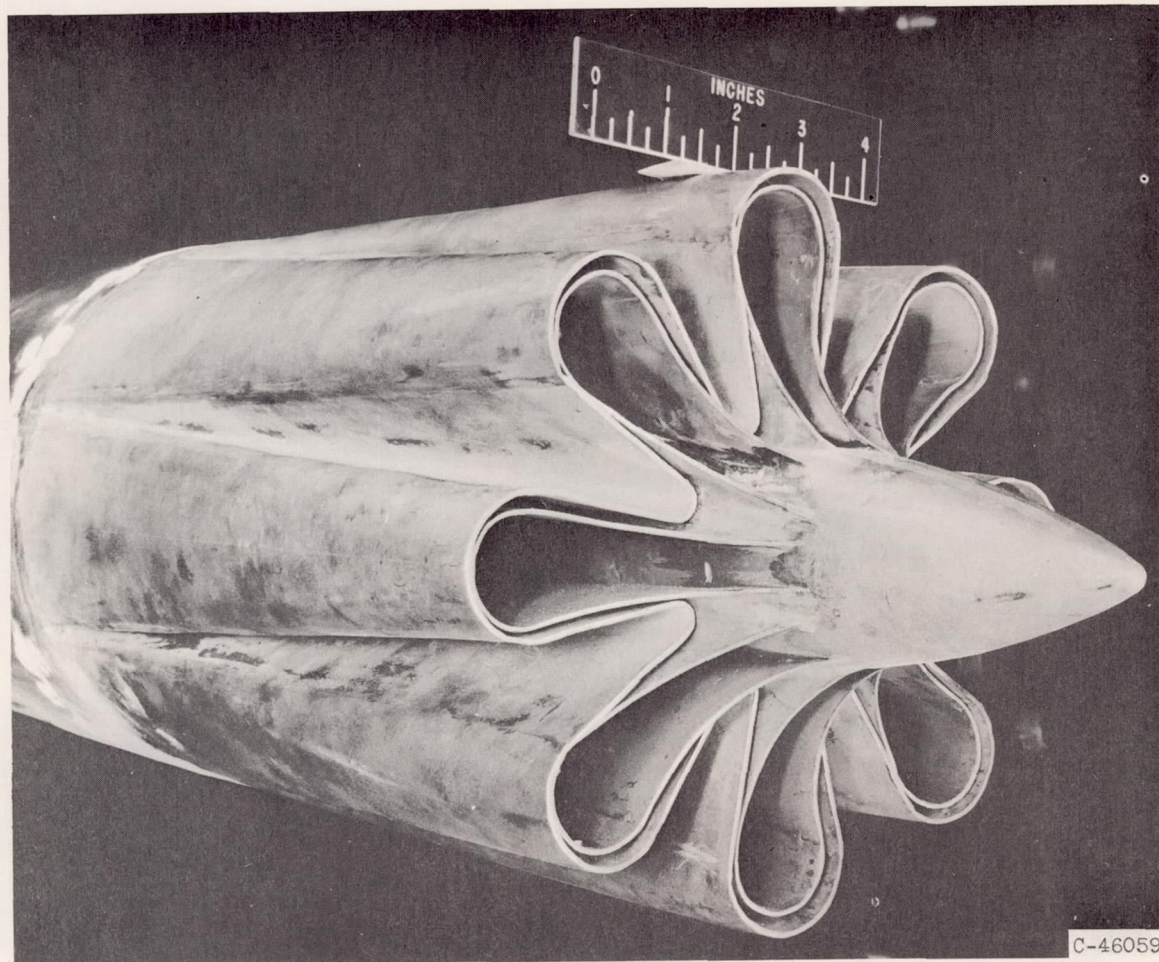


CD-5988

(c) Nine-tube configuration.

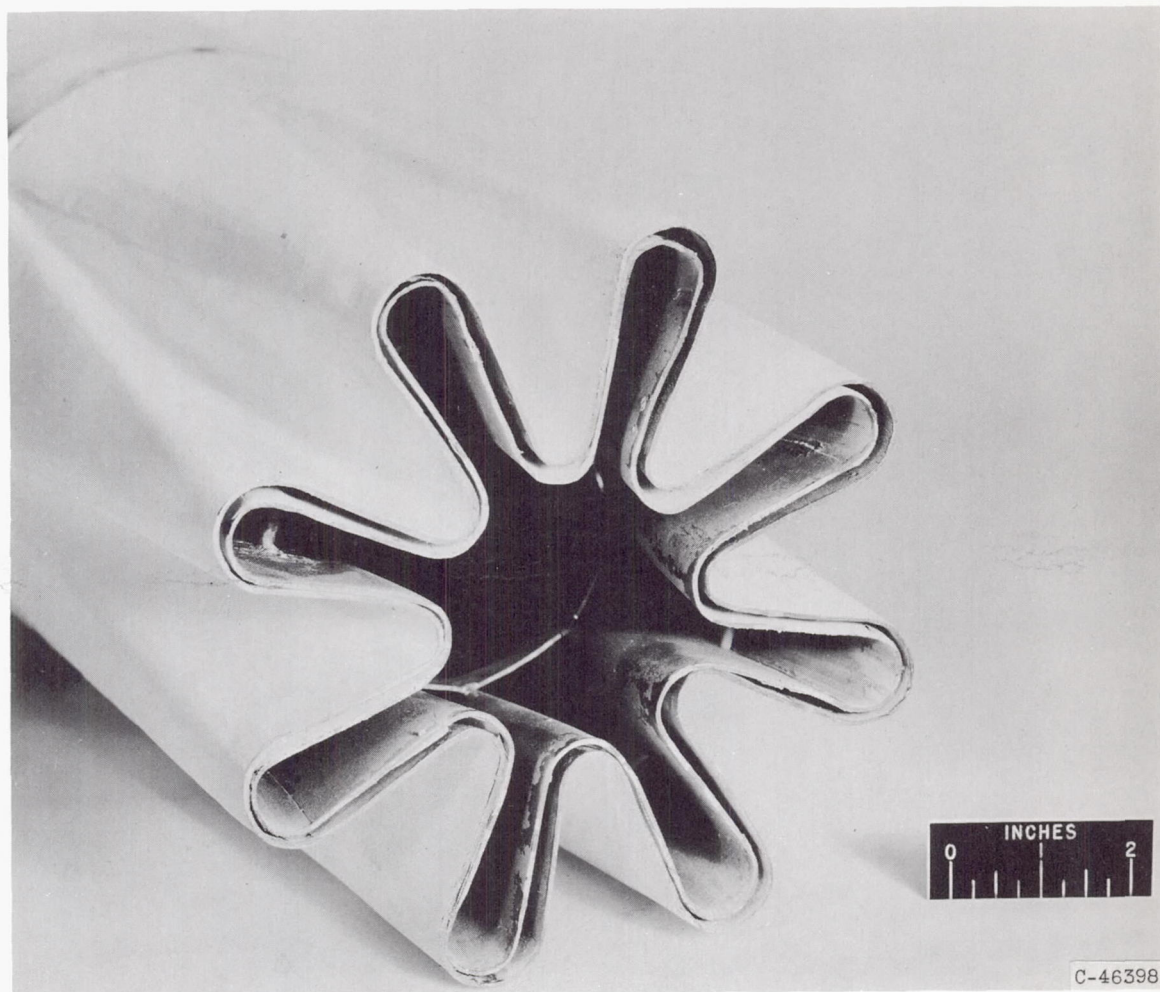
Figure 3. - Continued. Nozzle details.

4838

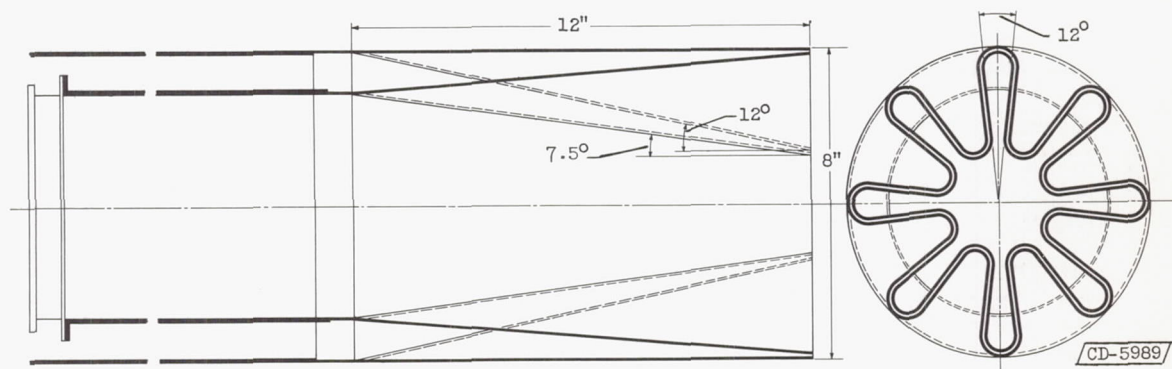


(d) Eight-lobe nozzle with centerbody.

Figure 3. - Continued. Nozzle details.

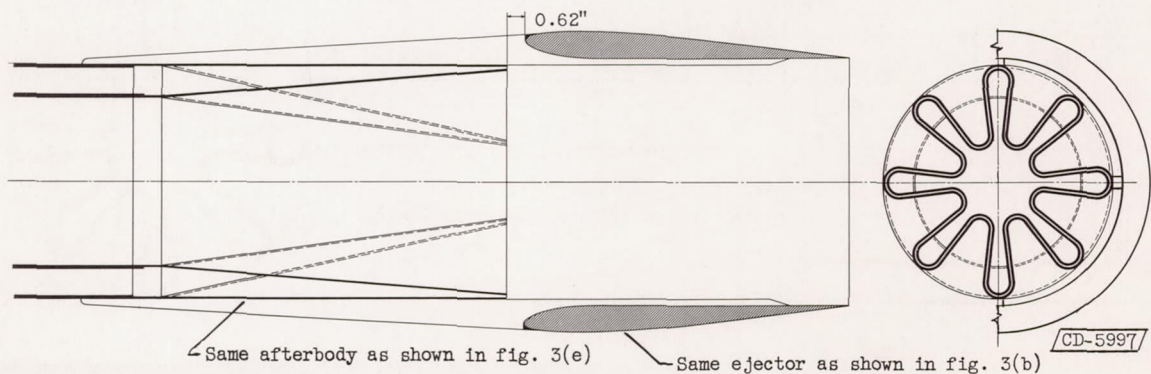
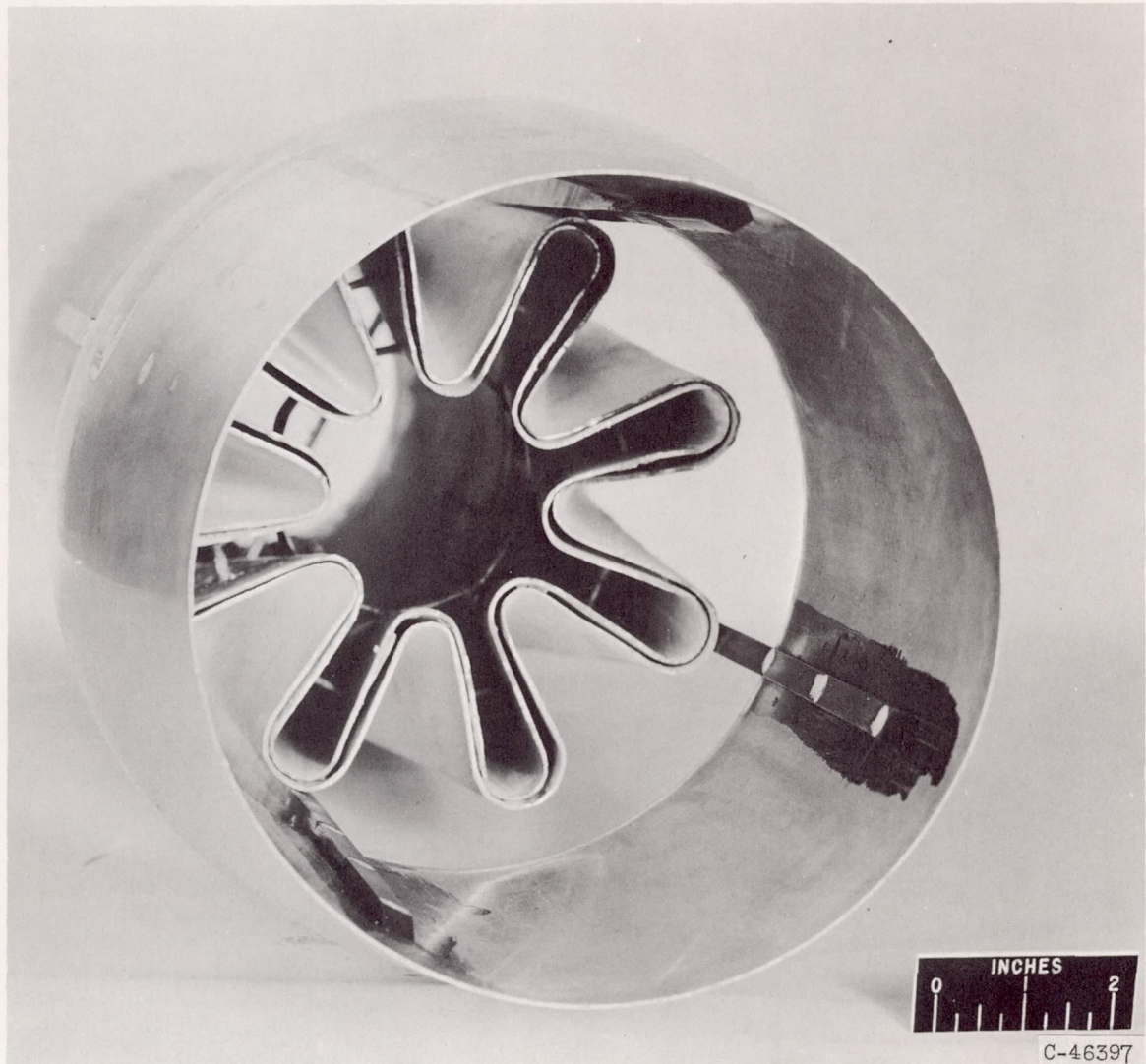


C-46398



(e) Eight-lobe nozzle.

Figure 3. - Continued. Nozzle details.



(F) Eight-lobe nozzle with ejector.

Figure 3. - Concluded. Nozzle details.

4838

CP-3

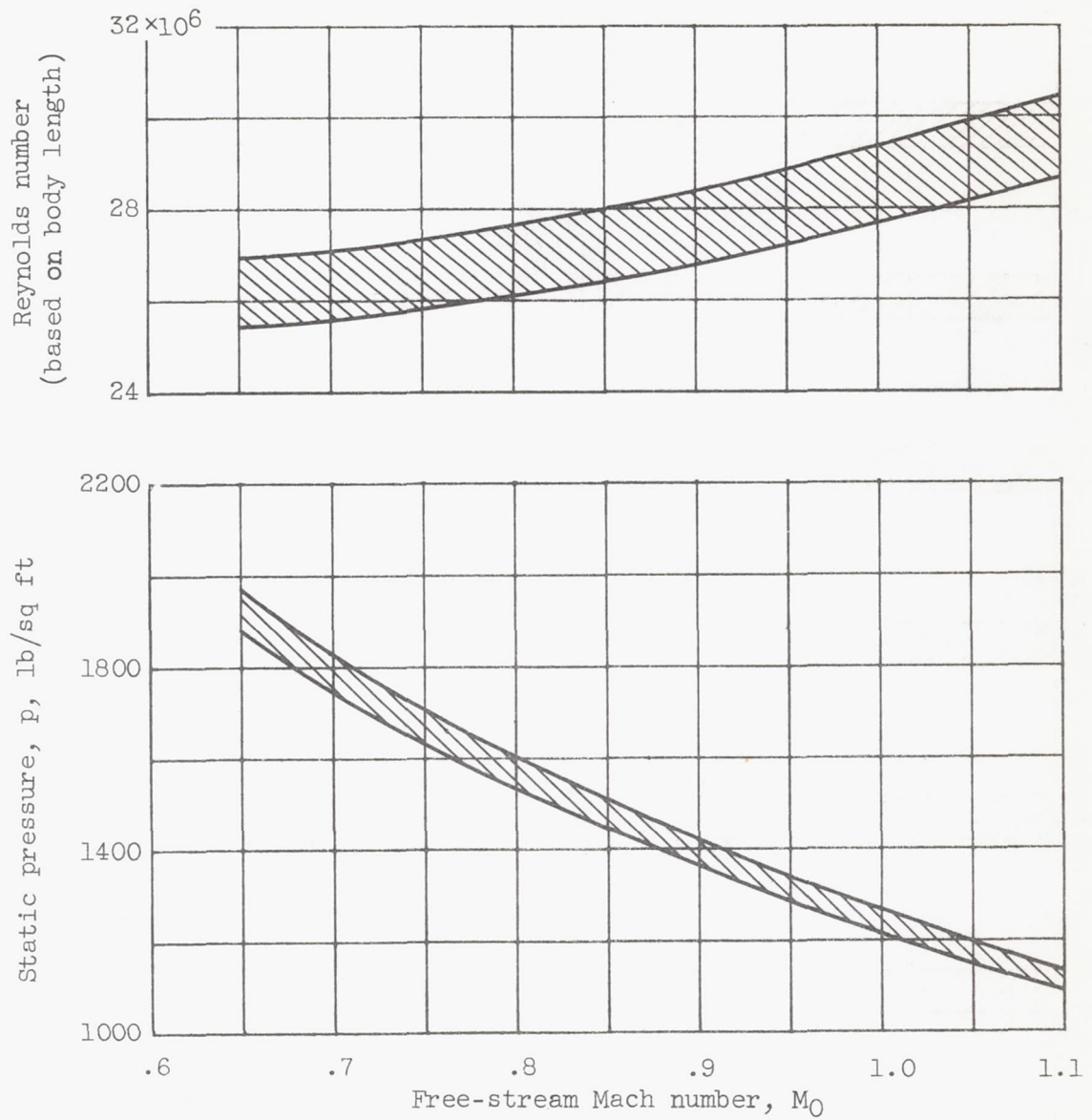


Figure 4. - Wind-tunnel test conditions.

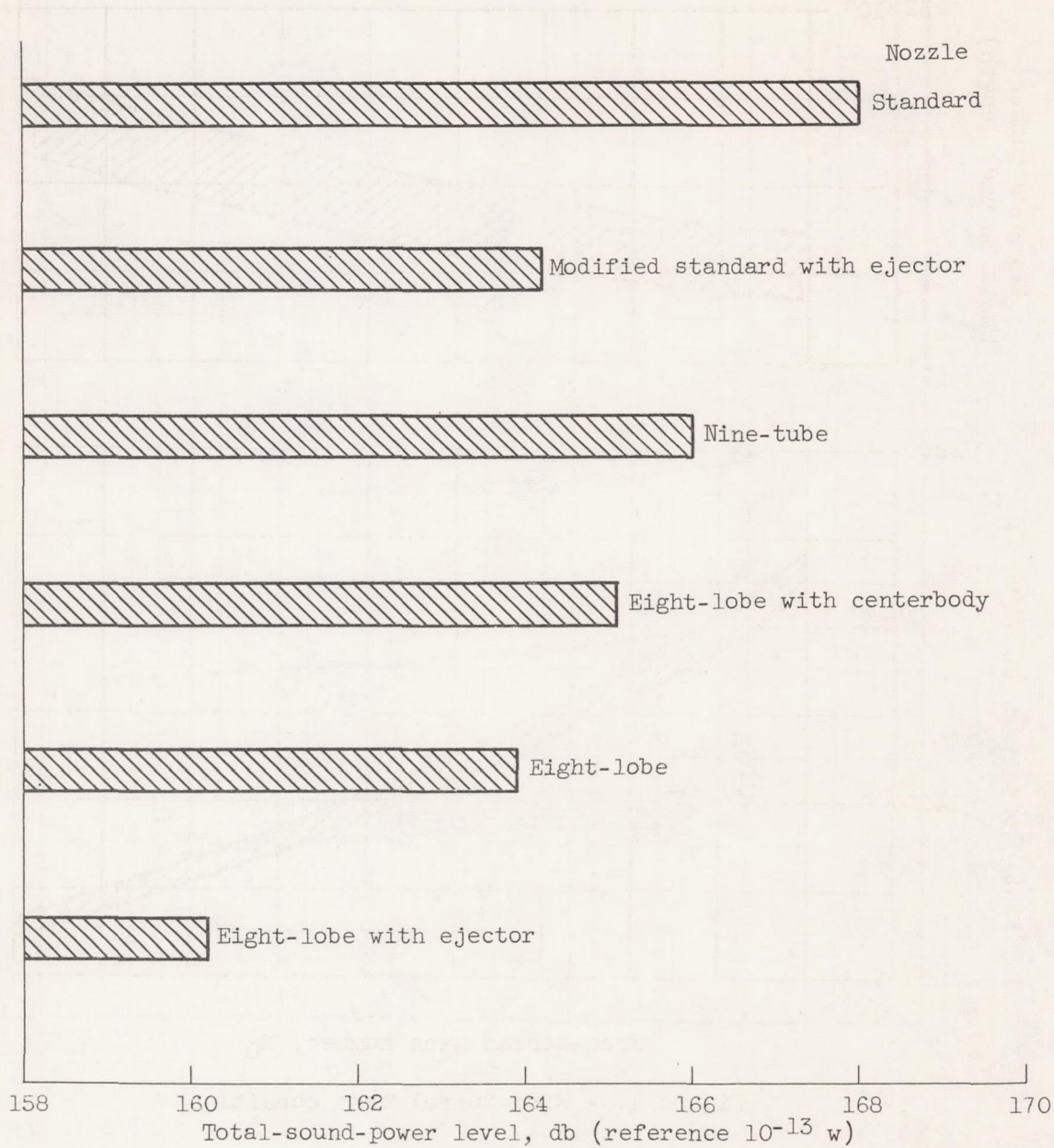
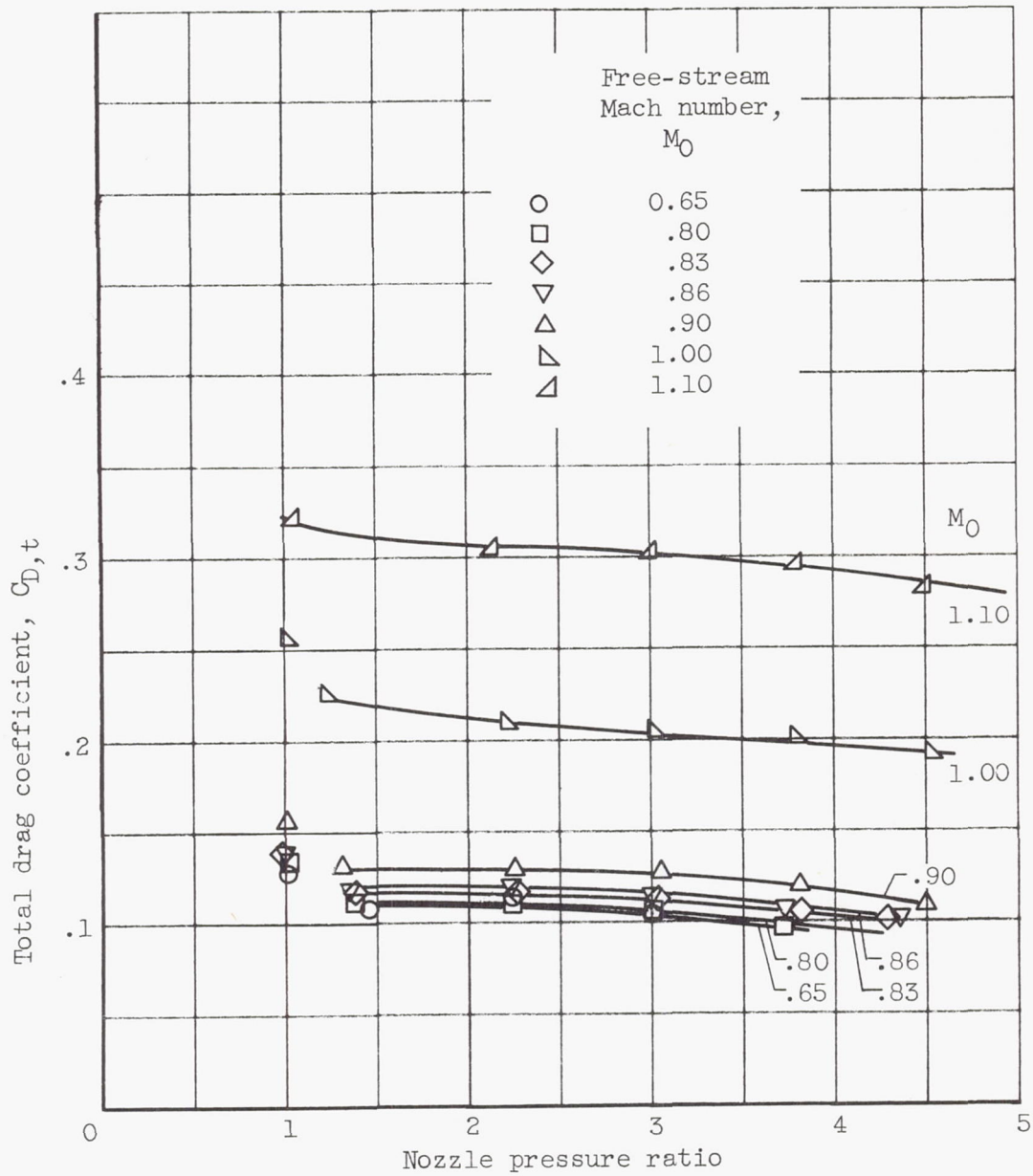
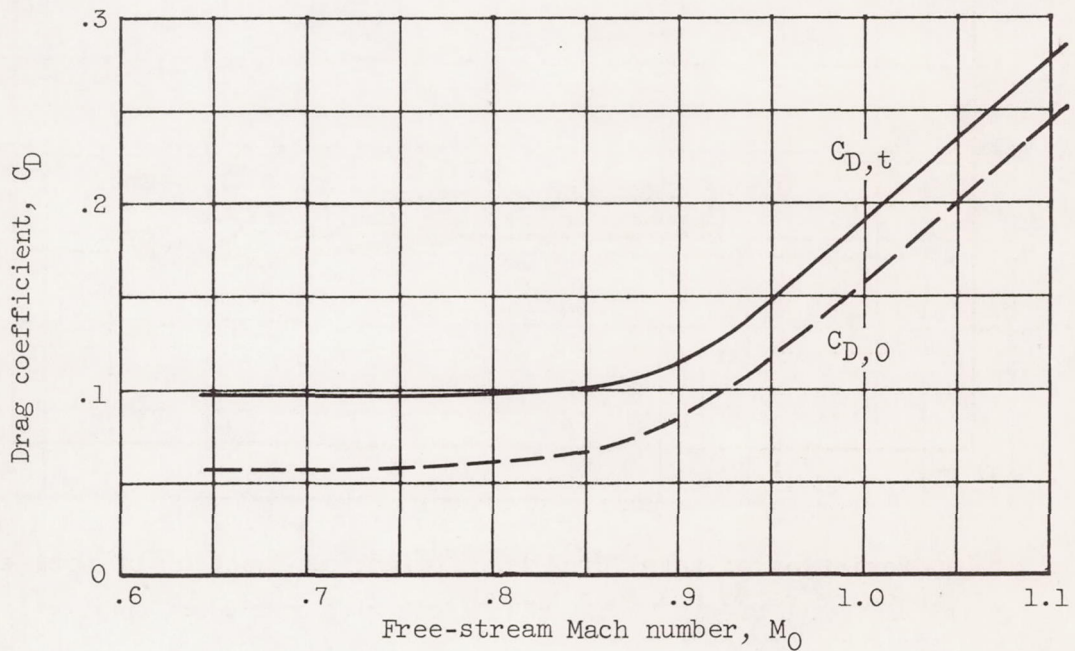
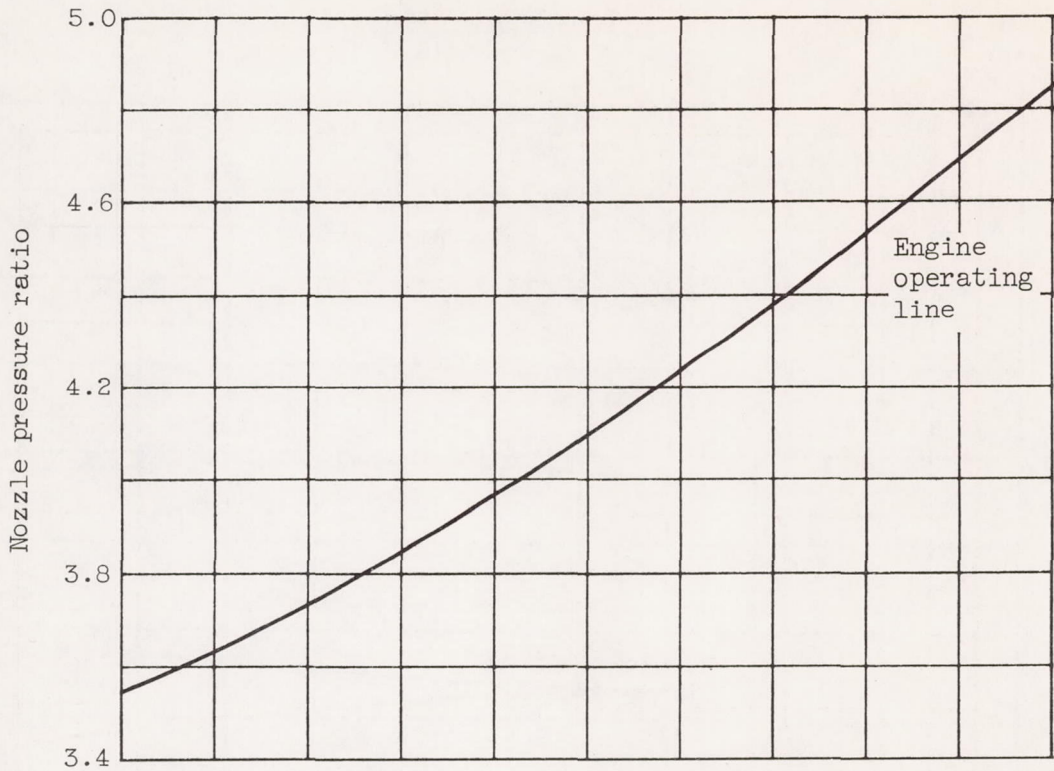


Figure 5. - Total-sound-power comparison at thrust of 7500 pounds.



(a) Variation of total drag coefficient as function of nozzle pressure ratio and Mach number.

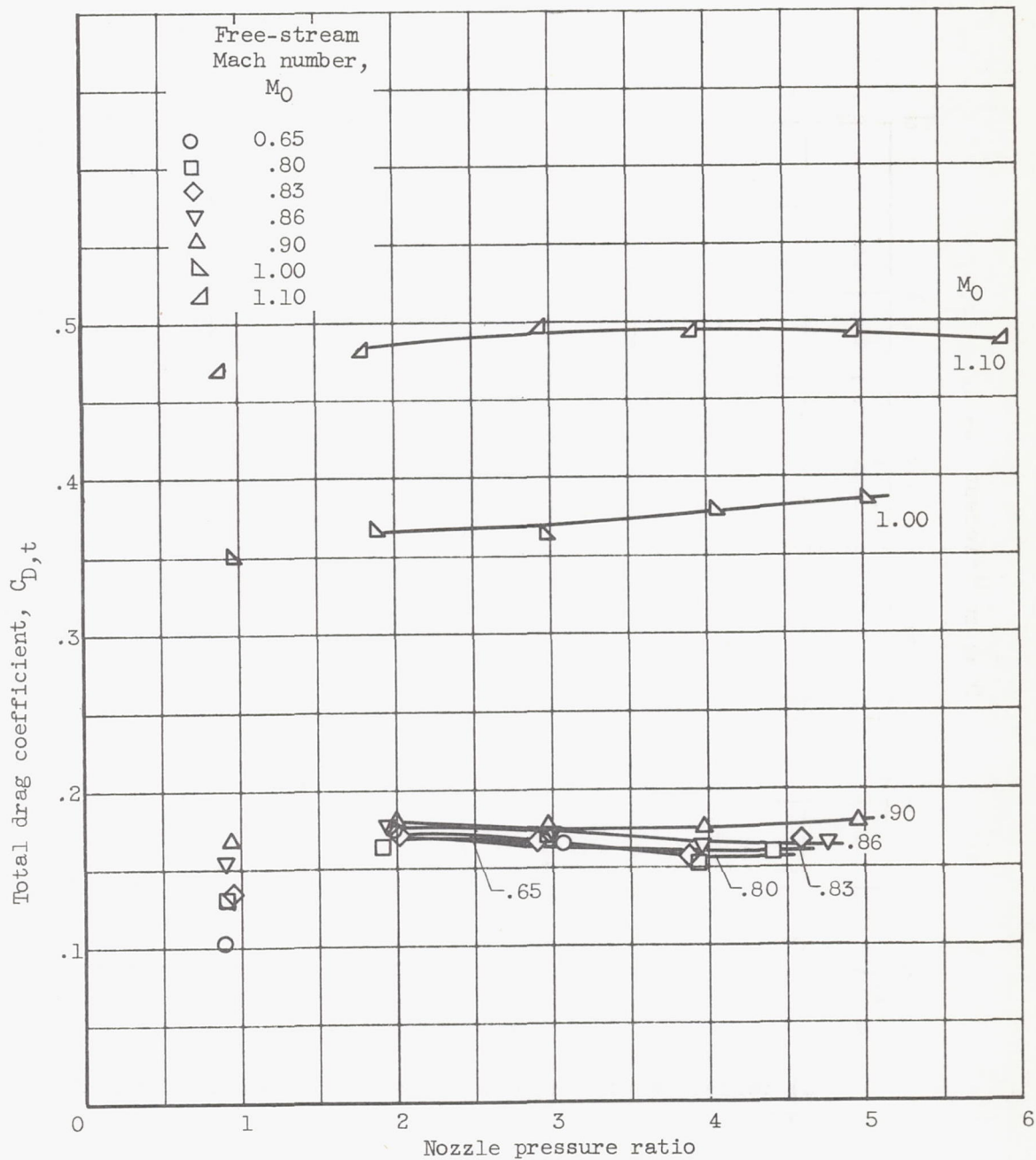
Figure 6. - Standard nozzle.



(b) Variation of component drag coefficient with Mach number.

Figure 6. - Concluded. Standard nozzle.

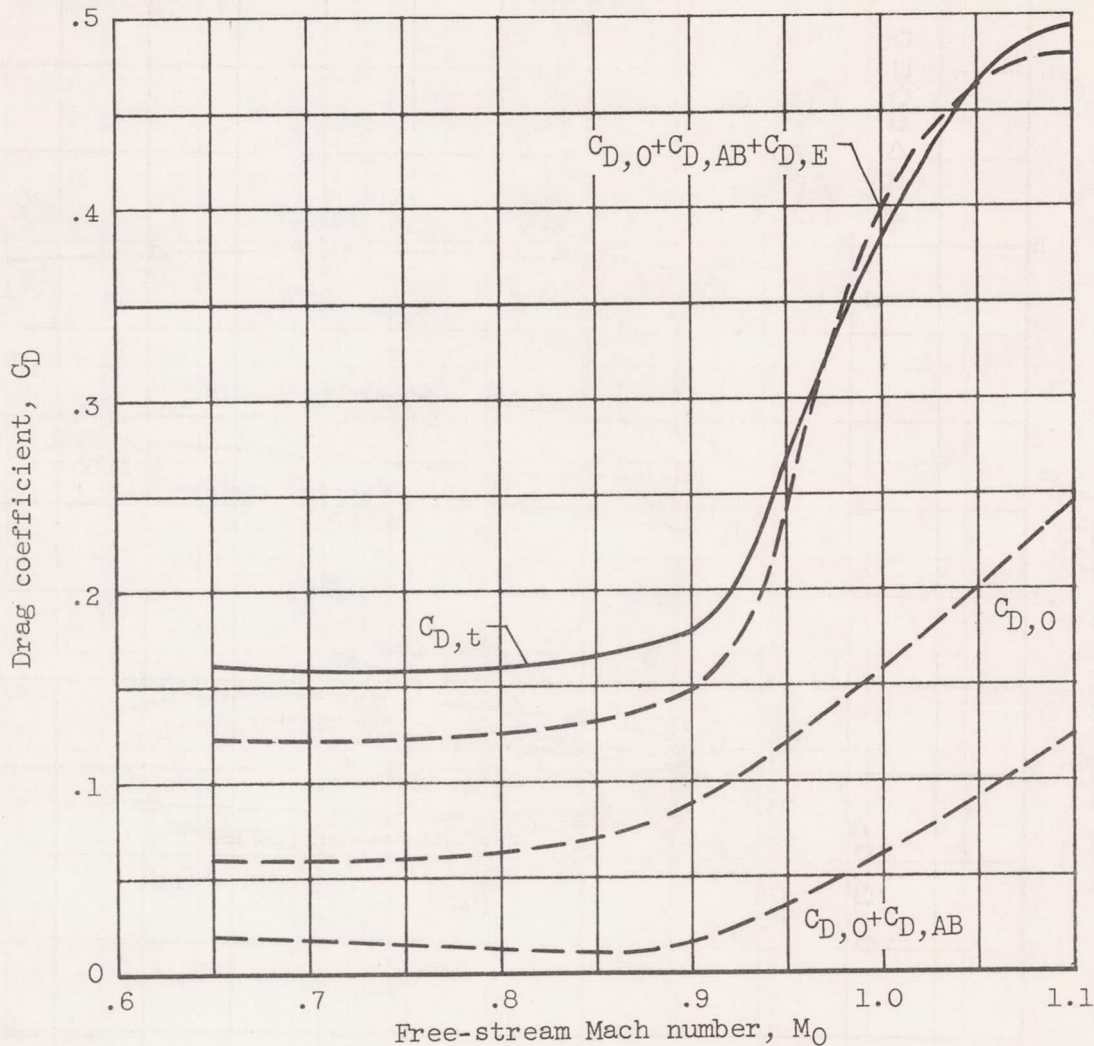
4838



(a) Variation of total drag coefficient with nozzle pressure ratio and Mach number.

Figure 7. - Standard nozzle with ejector.

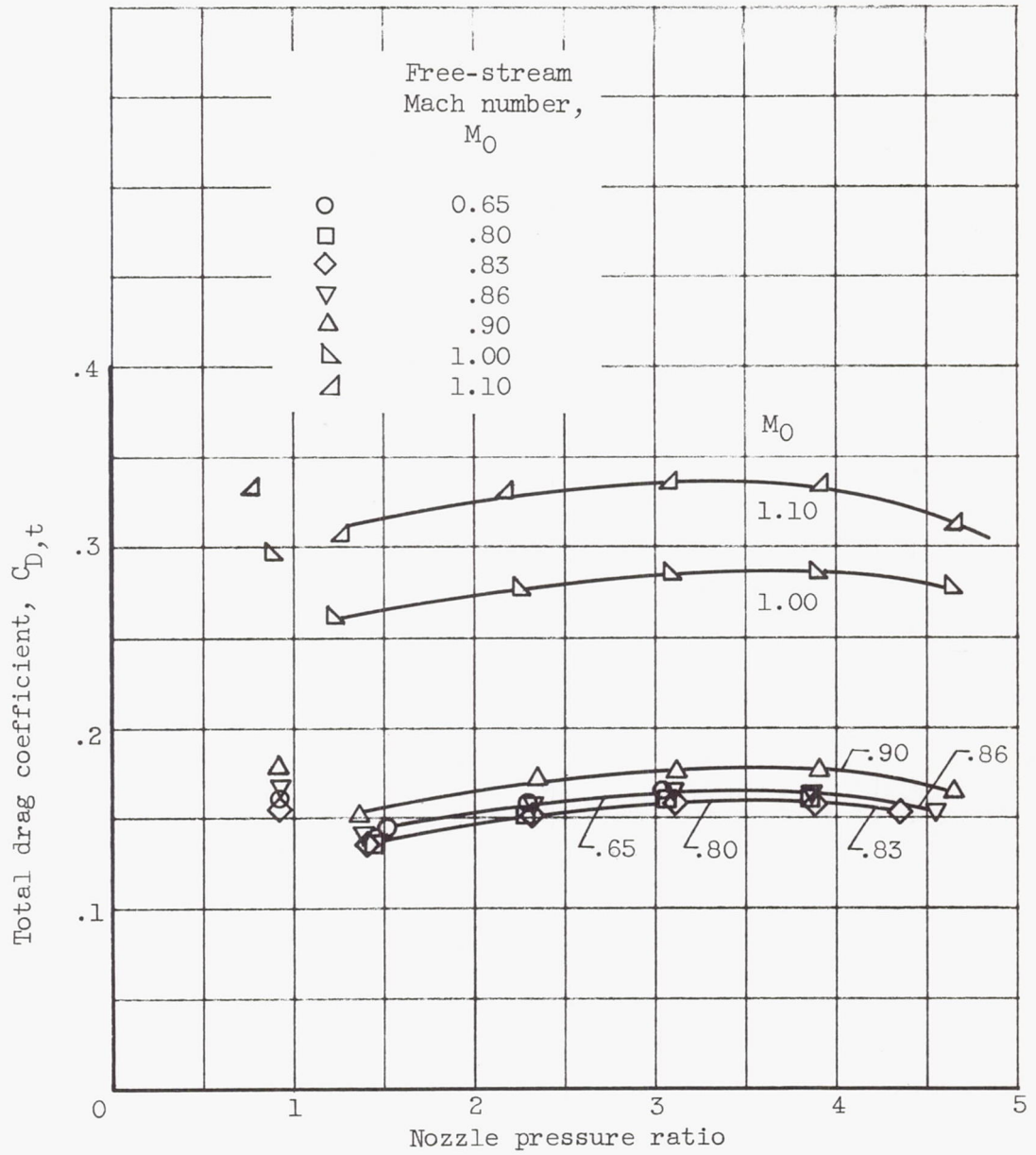
4838



(b) Variation of component drag coefficients with Mach number.

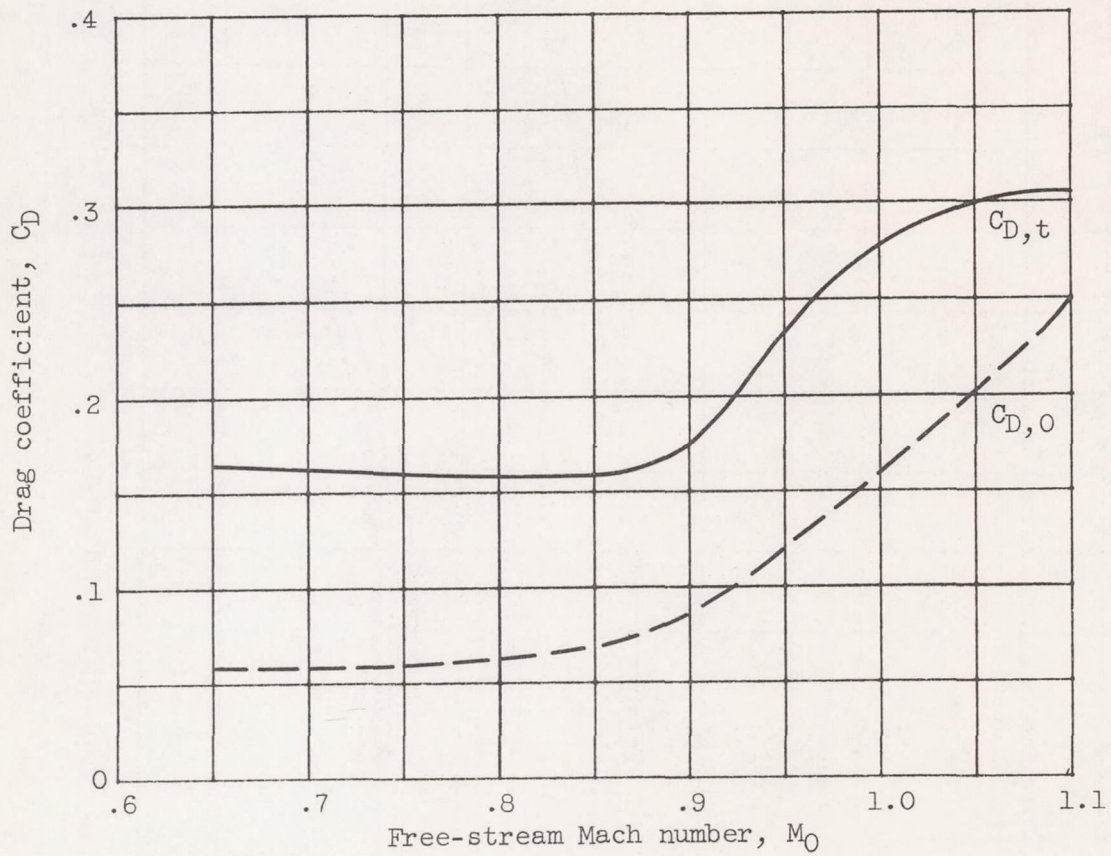
Figure 7. - Concluded. Standard nozzle with ejector.

4838



(a) Variation of total drag coefficient with nozzle pressure ratio and Mach number.

Figure 8. - Nine-tube nozzle.

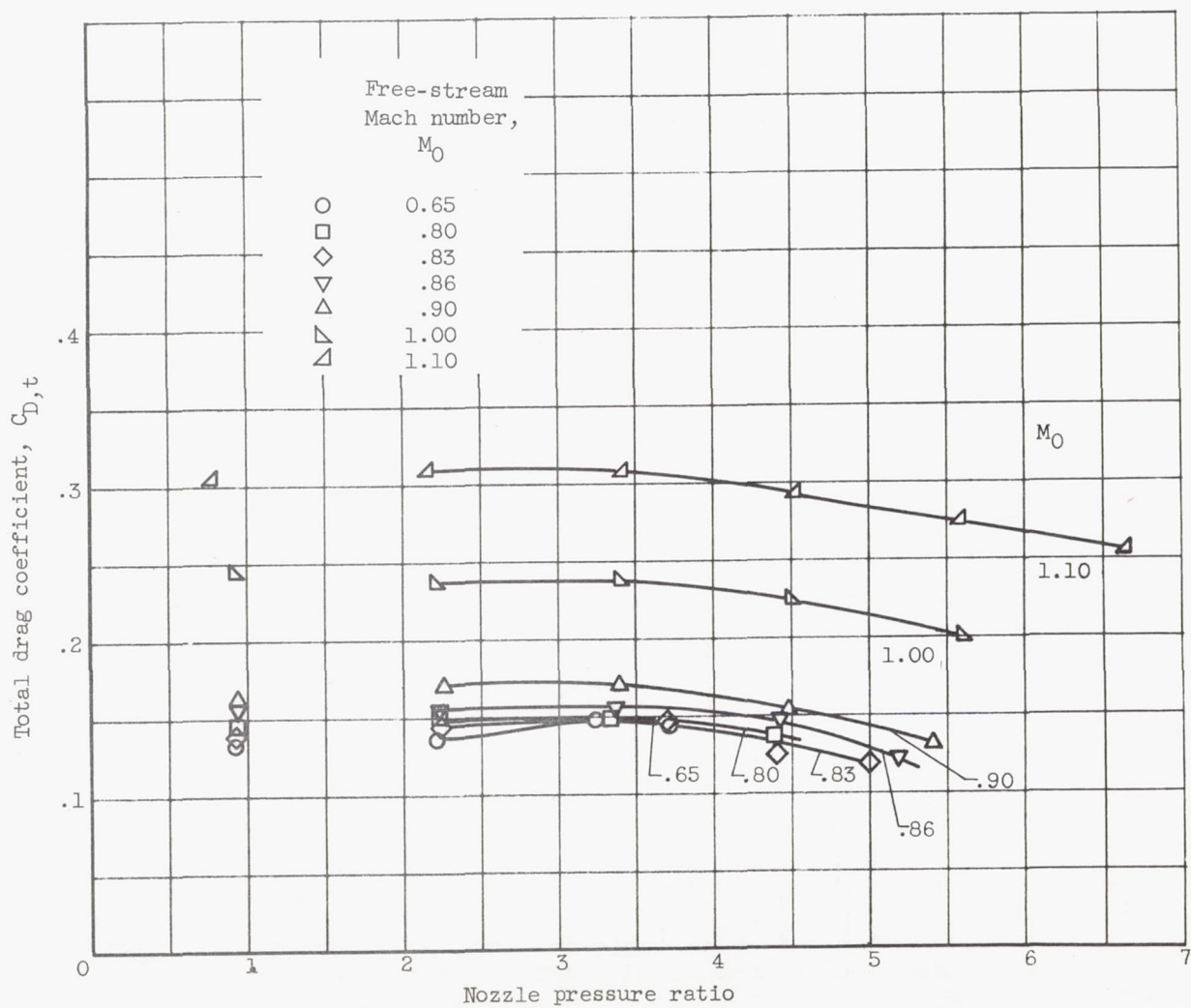


(b) Variation of component drag coefficients with Mach number.

Figure 8. - Concluded. Nine-tube nozzle.

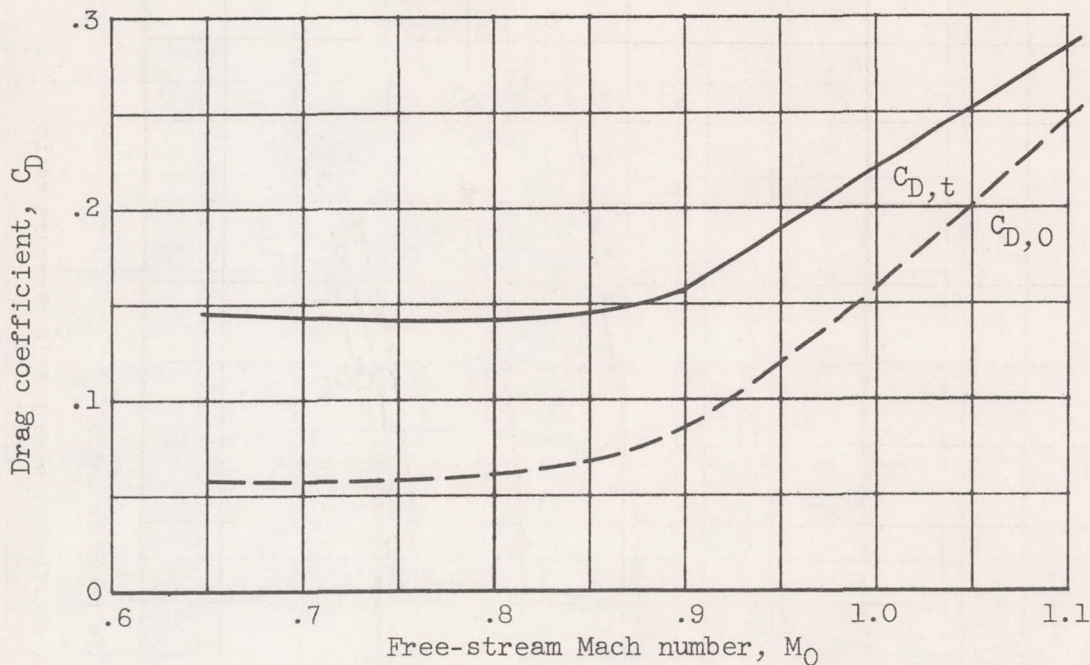
4838

CP-4



(a) Variation of total drag coefficient with nozzle pressure ratio and Mach number.

Figure 9. - Eight-lobe nozzle with centerbody.

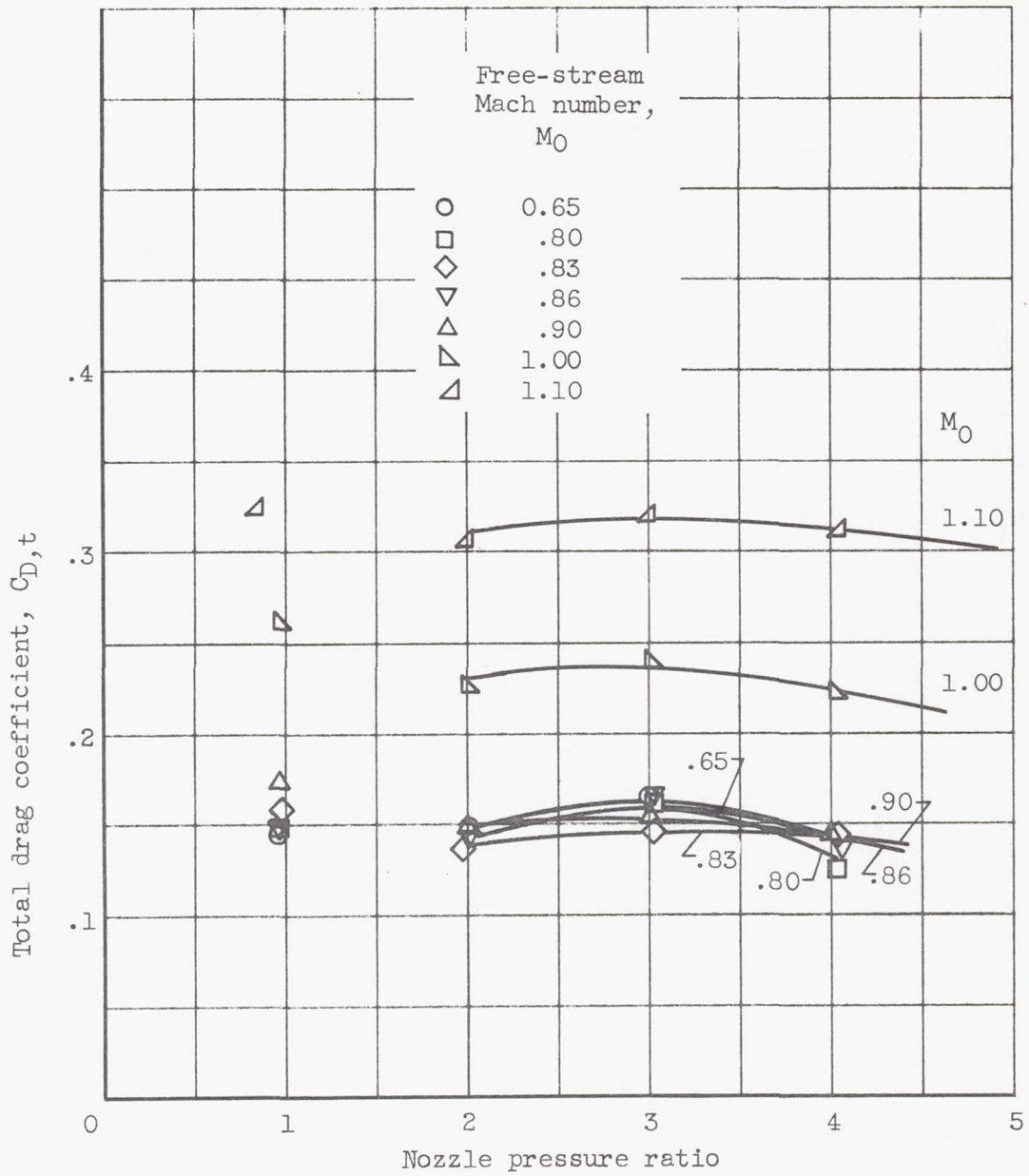


(b) Variation of component drag coefficients with Mach number.

Figure 9. - Concluded. Eight-lobe nozzle with centerbody.

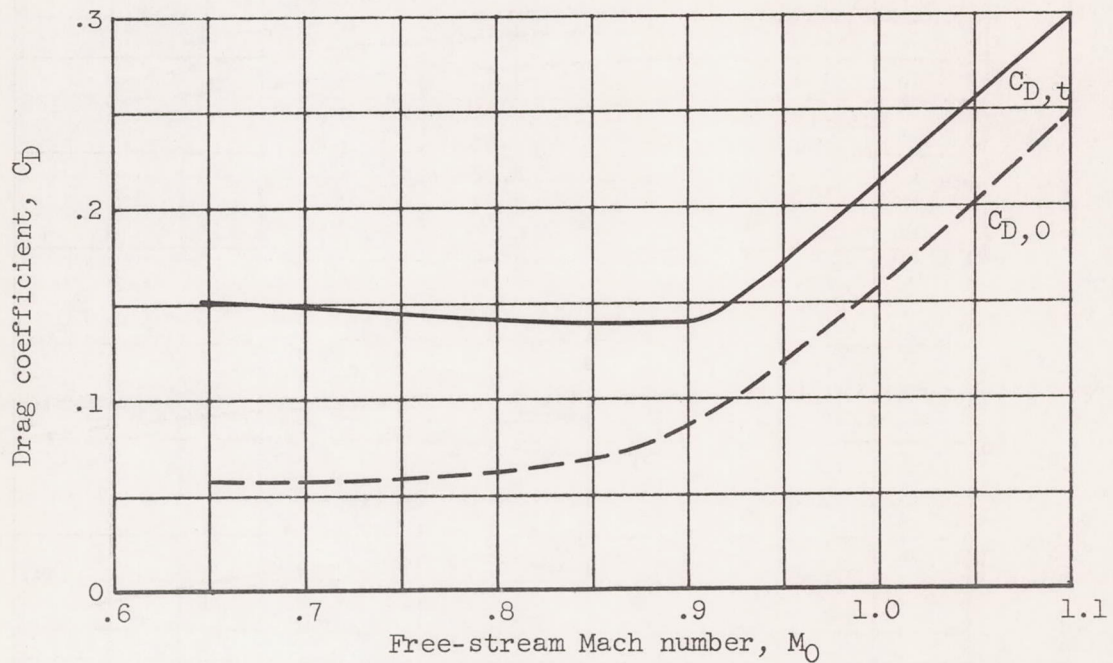
4838

CP-4 back



(a) Variation of total drag coefficient with nozzle pressure ratio and Mach number.

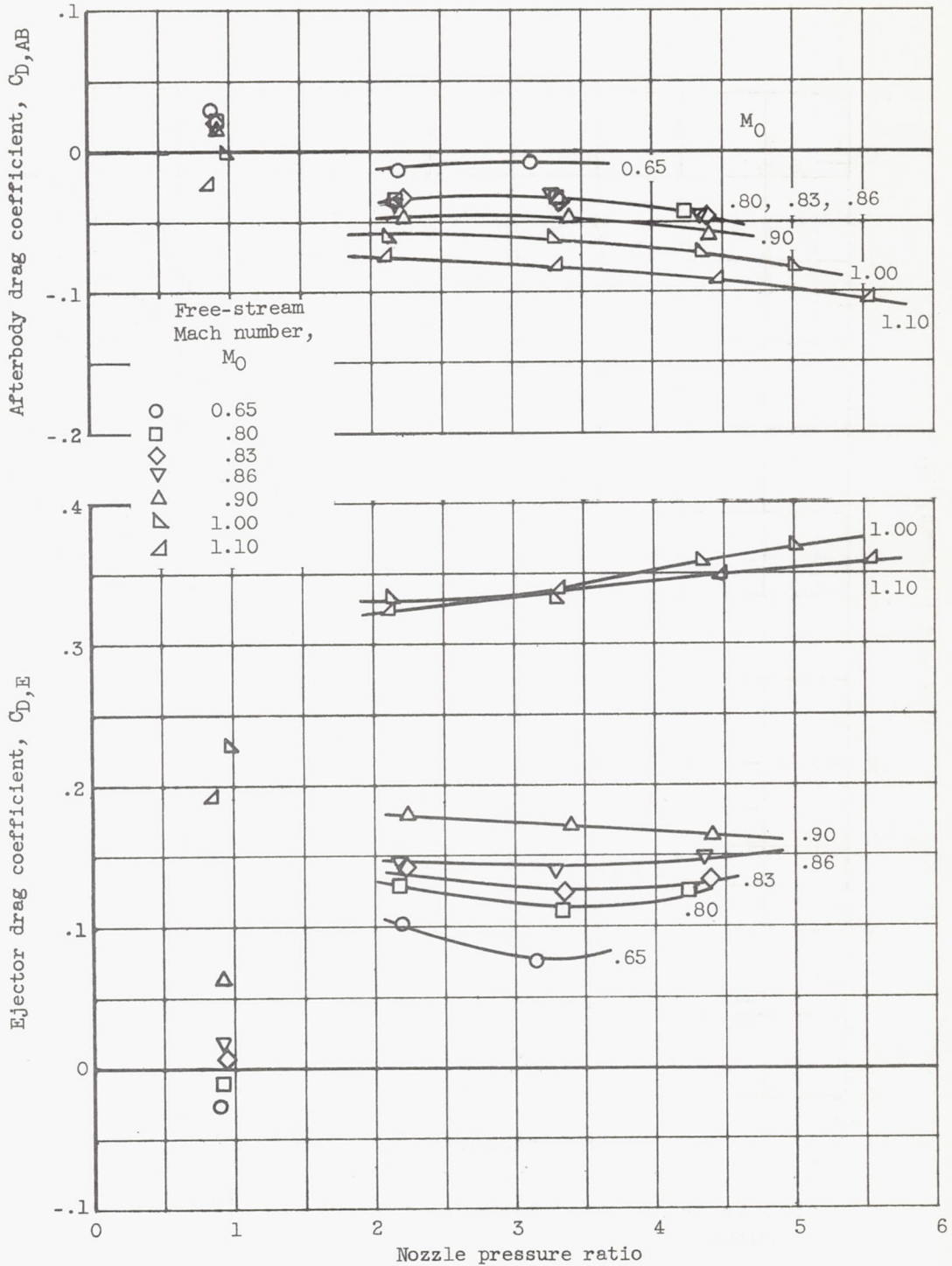
Figure 10. - Eight-lobe nozzle.



(b) Variation of component drag coefficients with Mach number.

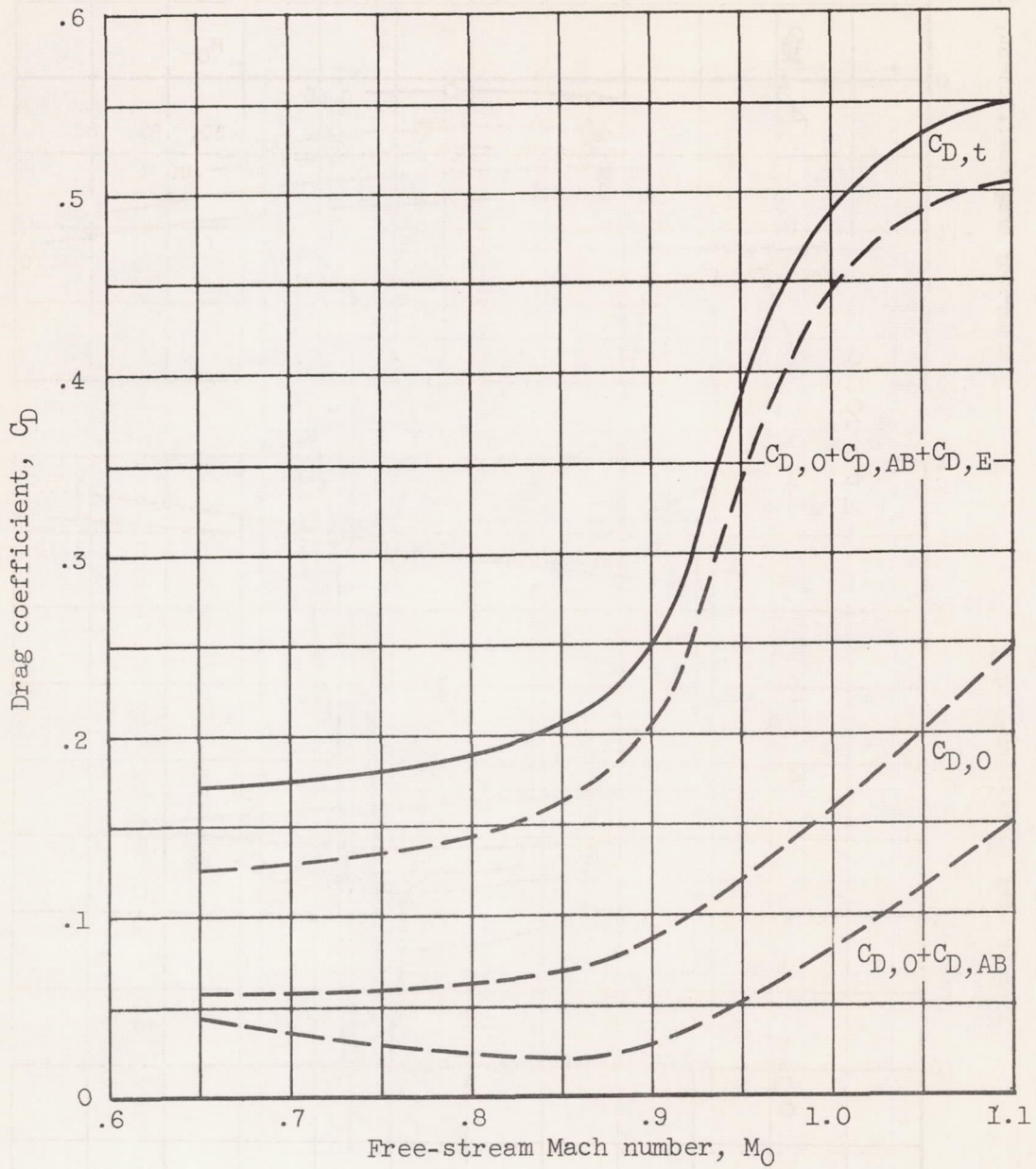
Figure 10. - Concluded. Eight-lobe nozzle.

4838



(a) Variation of ejector and afterbody pressure drag coefficients with nozzle pressure ratio and Mach number.

Figure 11. - Eight-lobe nozzle with ejector.



(b) Variation of component drag coefficients with Mach number.

Figure 11. - Concluded. Eight-lobe nozzle with ejector.

4838

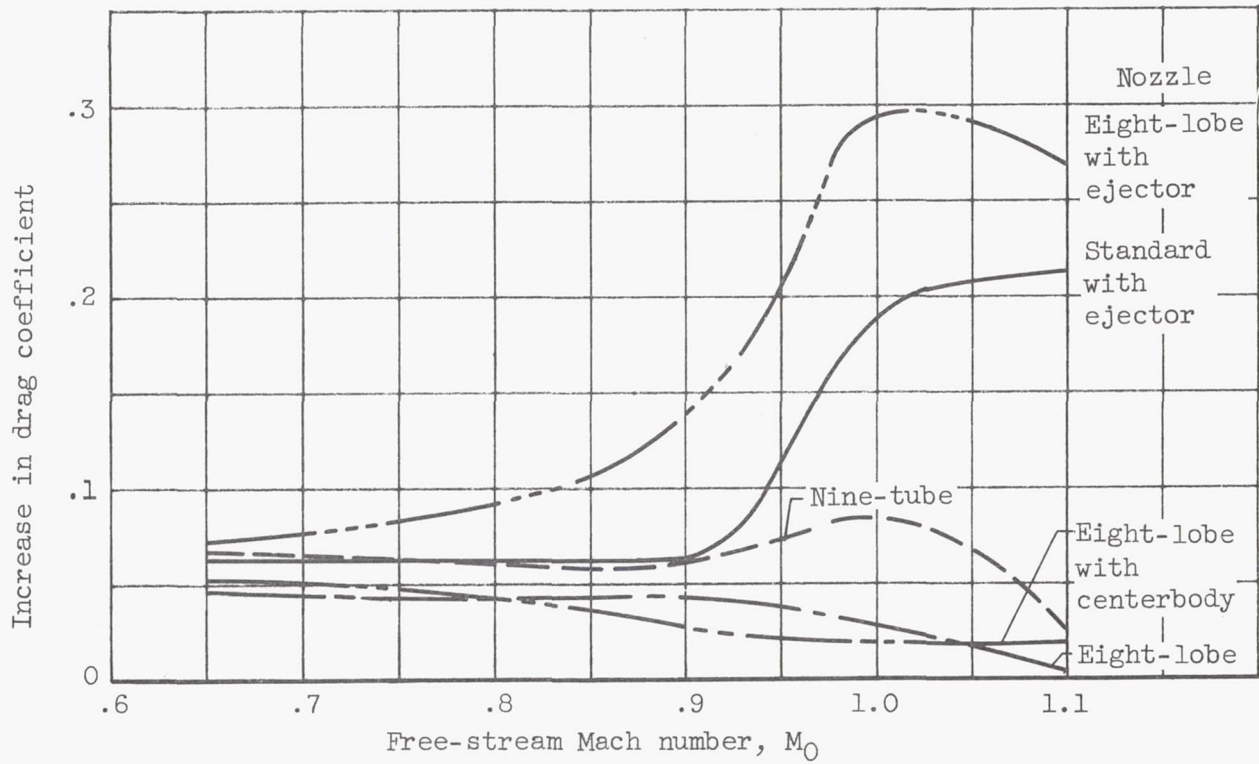


Figure 12. - Increase in drag coefficient over that of standard-nozzle configuration.

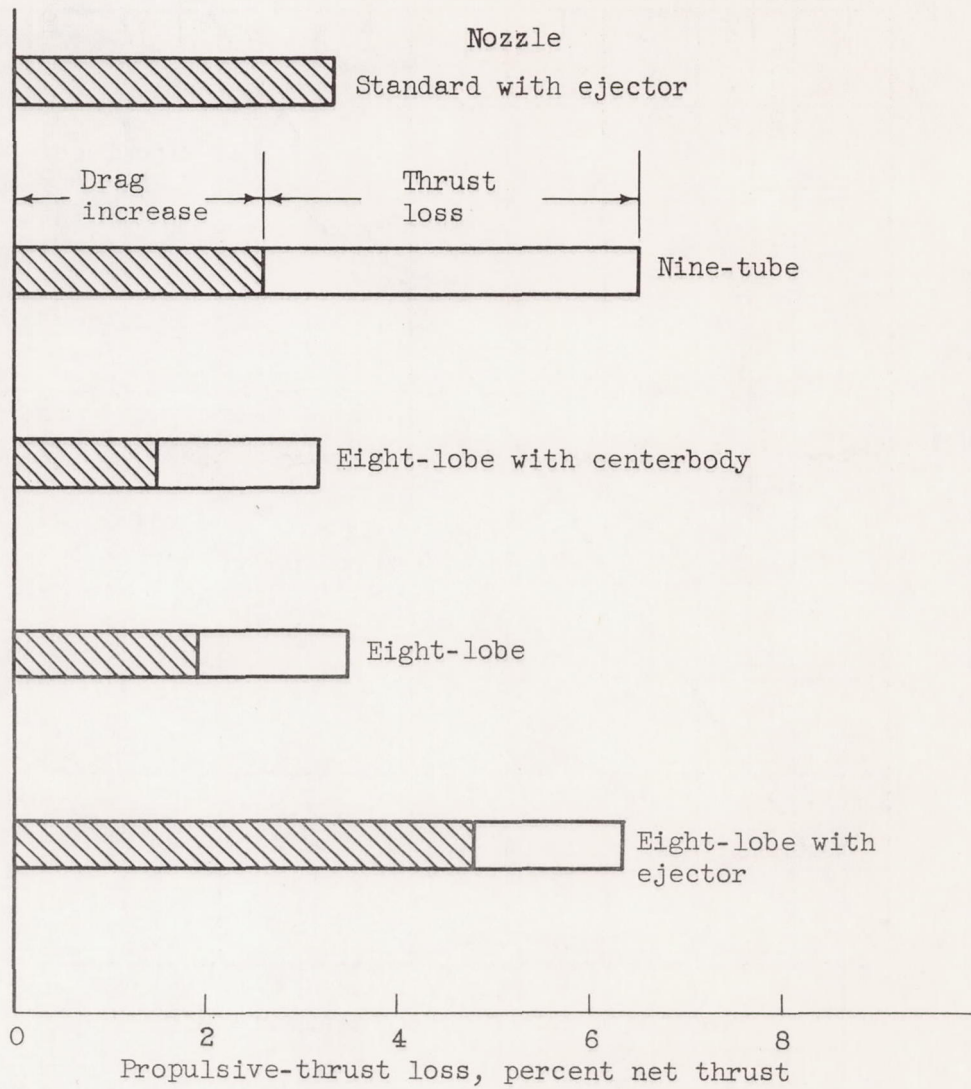


Figure 13. - Propulsive-thrust comparison at Mach number 0.86.

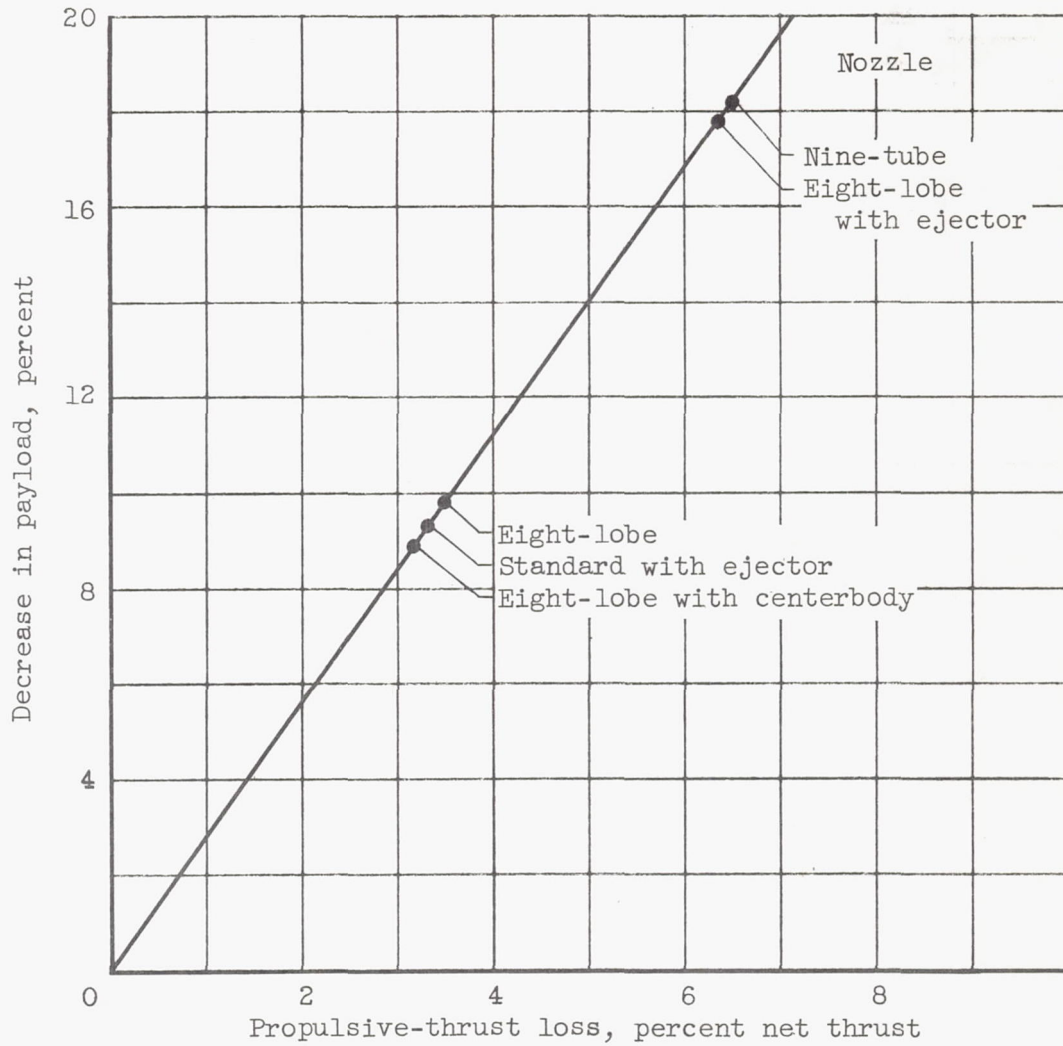


Figure 14. - Effect of propulsive-thrust loss on payload for 3500-mile range.